Supplementary Materials for

Potent Protection Against H5N1 and H7N9 Influenza via Childhood Hemagglutinin Imprinting

Katelyn M. Gostic, Monique Ambrose, Michael Worobey, and James O. Lloyd-Smith

correspondence to: worobey@email.arizona.edu or jlloydsmith@ucla.edu

This PDF file includes:

Materials and Methods
Supplementary Text
Figs. S1 to S12
Tables S1 to S2
Captions for databases S1 to S3

Other Supplementary Materials for this manuscript includes the following:

Databases S1 to S3 as zipped archives:
- H5N1 line list
- H7N9 line list
- Code for model comparison

Materials and Methods

Case data

We compiled data describing all reported human cases of H7N9 (2013-Nov. 2015) and H5N1 (1997-Nov. 2015) influenza. We obtained case data from three previously published H5N1 line lists, one spanning 1997 *(35)* and the other spanning Sept. 2006-Aug. 2010 *(36)*. We obtained data from one H7N9 line list spanning Jan.-Sept. 2013 *(37)*. For all other cases, we compiled original line lists using reports from the WHO as our primary resource and the Hong Kong Centre for Health Protection as a secondary resource. We incorporated additional cases or case details from Flu Trackers (https://flutrackers.com/forum/). Our newly compiled line lists are available as supplementary data files. Hyperlinks to information sources for each case are provided within.

We included confirmed, suspected and probable cases in our final analysis, but verified that our results are robust to the exclusion of unconfirmed cases (Fig. S7). We excluded cases for which patient age was not reported. Our H7N9 database contained 686 confirmed, suspected or probable cases, which were reported between April 1, 2013 and Nov. 13, 2015. All occurred in China. We excluded 6 cases for which patient age was not available, and used the remaining 680 cases, including 132 deaths, in our analysis (676 were confirmed and 4 were suspected or probable). In the same time period, WHO reported 681 confirmed cases of H7N9, so at most we are missing information on 5 confirmed cases (or fewer if some of these cases were included among our suspected and probable cases).

In total, our H5N1 database contained 927 confirmed, suspected or probable cases. These cases were reported in the 1997 Hong Kong outbreak, or in any country globally between Feb. 19, 2003 and Nov. 13, 2015. Over 94% of H5N1 cases occurred in Cambodia, China, Egypt, Indonesia, Thailand, and Vietnam, so we focused on these six countries and excluded 54 cases that occurred elsewhere. From the remaining 873 cases, we excluded an additional 38 cases for which patient age was not reported. Thus, we analyzed a total of 835 H5N1 cases, including 440 deaths (755 were confirmed and 80 were suspected or probable). In the same time period, WHO reported 823 confirmed cases of H5N1 in our study's six countries of interest, so at most we are missing information on 68 confirmed cases. Most of these additional confirmed cases were included in aggregate reports of H5N1 cases that lacked any accompanying details, making it impossible to determine whether case details reported elsewhere should be linked to WHO-confirmed case reports. Thus, it is possible that some of these WHO-confirmed cases were included in our database (based on information from Flu Trackers or other sources), but were listed as suspected or probable.

Mild or asymptomatic cases of both infections may not be ascertained *(1)*, so our results should be interpreted only as predictors of severe, symptomatic infection. We used simulated data to verify that our study's core findings should be robust to case ascertainment biases (see Supplementary Text, section 7).

Normalization of data to demographic age distribution

If all birth years were at equal risk of severe infection, we would expect the observed age distribution of cases to be proportional to the demographic age distribution. To examine excess incidence of severe infection or death, relative to this demographic null expectation, we normalized the observed data to the demographic age distribution (Fig. 2C, D). We tabulated the observed and expected number of cases occurring in each birth year, i, for each country, c, in each case observation year, y. To determine birth year, we subtracted case age from the year in which case onset occurred. To estimate the expected number of cases in each birth year, Exp_{yci} we used the following formula:

$$Exp_{yci} = D_{yci} I_{Total,yc} \quad (1)$$

Here D_{yci} describes the fraction of the total population, in country c, year y, that belongs to birth year i. $I_{Total,yc}$ describes the total number of cases or fatalities that occurred in year y, country c.

Finally, we defined normalized values within each birth year, N_i, as the unweighted sum, across all possible country-years, of differences between observed and expected numbers of cases or fatalities:

$$N_i = \sum_y \sum_c (Obs_{yci} - Exp_{yci}) \quad (2)$$

Model formulation

We used multinomial models to describe the probability distribution of H5N1 or H7N9 cases or fatalities across birth years. The multinomial distribution requires a set of parameters, p_{yci}, which described the probability that an infection observed in year y, country c, occurred in birth cohort i. Within each model, a unique combination of factors, including age-based risk of severe infection, poultry exposure risk, HA imprinting, and NA imprinting, determined p_{yci}. For each virus (H5N1 and H7N9), we fitted models independently for each case outcome (infection or death).

For each candidate model, we computed maximum likelihood parameter estimates to quantify the effects of relevant explanatory factors on birth-cohort risk (Table S1). Parameters H_m and N_m described the relative risk of severe infection or mortality for those with protective HA or NA imprinting, while parameters A_c and A_e described relative risk for young children (<5 years old) and the elderly (>65 years old).

We performed model comparison using AIC to determine which combination of factors best explained observed distributions of H5N1 or H7N9 incidence or mortality across birth years. We calculated Akaike weights, w_z, which can be interpreted as the proportional evidence in support of model z as the best of all models tested. Weights are calculated using the expression, $w_z = \frac{e^{\left(\frac{-\Delta AIC_z}{2}\right)}}{\sum_z e^{\left(\frac{-\Delta AIC_z}{2}\right)}}$ *(38)*. In many cases, when we added NA imprinting to models already considering HA imprinting, the maximum likelihood estimate of the N_m parameter was 1. In these cases, NA imprinting had no effect, and the new, more complex model became identical to the simpler model. We excluded these degenerate models from Akaike weight calculations.

Factors tested

Demography (D)

If all individuals were at equal risk of infection, regardless of birth year, the number of cases occurring in a given birth year would be proportional to the fraction of the population born in that year, as given by the country's demographic age distribution. Thus, for every country, c, and case observation year, y, a vector, D_{yc}, described the demographic age distribution and served as the null predictor of infection risk in each birth cohort. Vector D_{yc} was normalized to sum to 1, so that each element described the fraction of the population born in a particular year. Using the US Census Bureau's International Database *(39)*, we obtained publicly available demographic data for each country and year of case observation. Demography was included as a factor in every model tested (Supplementary Text).

Exposure to poultry (E)

Though limited human-to-human transmission is thought to occur, the majority of H7N9 and H5N1 infections are caused by spillover from infected poultry *(2, 6)*.To build models incorporating age-based patterns of exposure to poultry (E), we obtained published data from six surveys conducted in provinces that have experienced at least five cases of H5N1 or H7N9. These data were collected in three cities, Guangzhou, Shanghai and Shenzhen, and two non-urban locations, subrural Guangzhou and Xiuning, in China *(6, 7)*. Note that we included data from two independent surveys conducted in urban Guangzhou, for a total of six survey data sets. No poultry exposure data were available for other affected countries.

Although poultry exposure patterns vary by location, even within China, large reported uncertainties and geographic constraints on the available data prohibited a statistically valid effort to match cases with geographically specific exposure patterns. Instead we computed an average exposure rate for each birth cohort and year of H5N1 or H7N9 case observation, as follows. Each survey reported poultry exposure rates by age group. We used these values to assign each birth cohort an age-specific poultry exposure rate, based on their ages in each possible year of case observation. If exposure rates were not reported explicitly for young children, we substituted the rate reported for the youngest available age group. We then normalized across birth cohorts to determine the proportional risk of exposure at each survey location. Normalization ensured that survey locations reporting higher overall rates of exposure did not disproportionately influence model inputs. Finally, for each birth year, we took the average proportional exposure rate across all six poultry exposure surveys. These normalized exposure scores are shown in Fig. S10 B.

Age-based risk of severe infection (A)

A basic principle of influenza epidemiology is that children under 5 and elderly adults over 65 are high-risk groups for severe influenza infection *(40-42)*. These groups may be more susceptible to severe influenza infections, or may seek healthcare at an increased rate, leading to case-ascertainment biases. Models including the age-based risk factor (A) introduced two parameters that allowed each high-risk age group to experience increased risk of severe infection relative to adults and children ages 5-64. Parameter A_c

quantified the relative risk of young children, while parameter A_e quantified the relative risk of the elderly (Table S1). Both parameters are constrained take a minimum value of 1 so as to represent elevated risk of severe infection.

For mortality analyses, we noted that case-fatality rates are not always elevated in children, despite their elevated risk of severe infection *(41)*. Thus, for mortality analyses we relaxed the constraint on parameter A_c, allowing the data to inform whether young children exhibit increased ($A_c > 1$) or decreased ($A_c < 1$) risk of death from H7N9 or H5N1 infections, relative to the general population.

Hemagglutinin imprinting (H)

Models that considered hemagglutinin imprinting (H) divided the population into two exposure groups: those with group-matched first IAV exposures (protective HA imprinting), and all others (non-protective HA imprinting or naïve children). We calculated the fraction of each birth cohort with first exposure to either HA group using methods described below (see Reconstructing immune imprinting patterns). We initially separated naïve children from adults with non-protective HA imprinting, but our results consistently indicated no difference in risk between these groups (results not shown), leading us to combine naïve children and mismatched HA imprinting into a single reference group.

Hemagglutinin imprinting models introduced a single parameter, H_m, which allowed the group with protective HA imprinting to experience decreased risk relative to all others in the population.

Neuraminidase imprinting (N)

As for HA imprinting, models that considered NA imprinting divided the population into two groups: one with matched (protective) first IAV exposures, and a reference group that included all others. Models containing factor N introduced one parameter, N_m, which allowed the group with protective NA imprinting to experience decreased risk. Two phylogenetic groups have been identified for NA, as for HA. We are not aware of experimental evidence of cross-protection between NA subtypes within the same phylogenetic group (without which NA history could not explain incidence patterns for H7N9, since N9 is not known to have circulated in the human population). However, given that N9 and N2 fall in the same NA group, we considered the possibility that imprinting on N2 might be protective against N9. H5N1 is clearly matched to seasonal H1N1, as they share the N1 subtype—so this analysis fully captures patterns of first exposure to N1, which have been proposed previously as a driver of H5N1's infection age distribution *(3, 4)*.

Models tested

We tested models that considered all possible combinations of the above four factors, as well as demographic age structure. Our full set of 16 models included: D, DE, DA, DH, DN, DNH, DAH, DAN, DANH, DEA, DEH, DEN, DEAH, DEAN, DENH, and DEANH. For each model, we fit relevant parameters to the appropriate data before performing model comparison. We repeated each model analysis using both incidence and mortality data for H7N9 and H5N1. See Supplementary Text for model equations and likelihood functions.

Reconstructing immune imprinting patterns

To inform hemagglutinin and neuraminidase imprinting models, we estimated the fraction of each birth cohort with first IAV exposure to seasonal subtypes H1N1, H2N2 or H3N2, and the fraction that remained naïve. We first used a truncated geometric model to estimate the baseline probability that first IAV infection occurs at a given age. Because age-seroprevalence studies report that 98-100% of children have been infected with IAV by age 12 *(20, 21, 43)*, we set 12 as the maximum possible age of first infection. Let ε_{ij} be the probability that an individual with birth year *i* has his or her first IAV infection in calendar year *j*. Then:

$$\varepsilon_{ij} = \frac{(1-a)^{j-i}a}{\sum_{j=i}^{i+12}(1-a)^{j-i}a} \quad (3)$$

where *a* is the annual probability of infection (the baseline annual attack rate on seronegative children), and *j* takes values from *i* to *i+12*. Using published age-seroprevalence data *(20, 21)*, the maximum likelihood estimate for *a* was 0.28 (95% CI 0.26-0.30), consistent with other IAV attack rates estimated in children *(43-45)*.

To account for variability in the annual attack rate between years, we compiled an index of IAV circulation intensity from 1918-2015 (Supplementary Text). We defined the scaled annual attack rate as $a_m = aI_m$, where *m* is the calendar year, I_m represents that year's intensity score and *a* represents the baseline annual attack rate estimated above.

Finally, we modified equation 3 to account for variable annual attack rates and the possibility that some children have not yet been exposed:

$$\varepsilon_{ij|y} = \begin{Bmatrix} \frac{a_j}{N_{i|y}} & i = j \\ \frac{\left[\prod_{k=i}^{j-1}(1-a_k)\right]a_j}{N_{i|y}} & i < j \leq i+12 \end{Bmatrix} \quad (4)$$

Here, $\varepsilon_{ij|y}$ is the probability that individuals in birth cohort *i* experienced their first infection in calendar year *j*, given that H5N1 or H7N9 case observation occurs in year *y*. Note that because birth cohorts are very large, the fraction of birth cohort *i* with first exposure in year *j* converges to probability $\varepsilon_{ij|y}$. The expression, $\frac{a_j}{N_{i|y}}$ represents the probability of infection in the first year of life (at age 0), and the expression, $\frac{\left[\prod_{k=i}^{j-1}(1-a_k)\right]a_j}{N_{i|y}}$ represents the probability of infection at ages 1-12. The normalizing factor, $N_{i|y}$, reflects the assumption that all individuals have had their first infection by age 12, and is used to ensure that all relevant probabilities for an age group sum to 1. It is taken as:

$$N_{i|y} = \begin{Bmatrix} a_i + \sum_{j=i+1}^{i+12}\left[\prod_{k=i}^{j-1}(1-a_k)\right]a_j & y \geq i+12 \\ 1 & y < i+12 \end{Bmatrix} \quad (5)$$

When the birth cohort is older than 12 in the year of observation, $N_{i|y}$ always falls within the range (0.98-1.00) and minimally affects the final outcome. For birth cohorts that are younger than 12 at the year of observation ($y<i+12$), normalization is not appropriate because some individuals in the age group have not had their first exposure; in these instances we set $N_{i|y} = 1$ and calculate the naïve fraction as the complement of the cumulative probability of first exposure (equation 7).

Finally, we combined the age of first infection probabilities with seasonal circulation patterns to determine the fraction of age group *i* with first exposure to subtype *S* in year *j* and country *c* ($w_{S,i|y,c}$). We scaled $\varepsilon_{ij|y}$ by the fraction $f_{S|j,c}$ of circulating IAVs belonging to subtype *S* (where *S* could represent H1N1, H3N2 or H2N2):

$$w_{S,i|y,c} = \sum_{j=i}^{y} f_{S|j,c}\varepsilon_{ij|y} \quad (6)$$

For birth cohorts younger than 12 in the year of case observation ($y<i+12$), a portion of the cohort had not yet experienced a first IAV exposure. The fraction of cohort *i* that remained naïve in year *y* was given by:

$$w_{n,i|y,c} = 1 - \sum_{j=i}^{y} \varepsilon_{ij|y} \quad (7)$$

Values of $f_{S|j,c}$ were determined by IAV circulation history, and for all *j*, $f_{H1N1|j,c} + f_{H2N2|j,c} + f_{H3N2|j,c} = 1$. Prior to 1977, a single IAV subtype circulated each year, and pandemic years marked circulation of a new seasonal subtype. Thus, in years 1918-1976, $f_{S|j,c}$ was set equal to 1 for the circulating subtype, and 0 for all other subtypes.

For years 1977-2015, when H1N1 and H3N2 have circulated simultaneously, we estimated $f_{S|j,c}$ using influenza surveillance data reported by WHO collaborating laboratories *(46, 47)*. For each year of interest, we defined relative incidence as follows: $\frac{Positive\ specimens\ of\ subtype\ S}{All\ positive\ specimens\ of\ subtype\ H1N1\ or\ H3N2}$. Whenever possible (1997-2015), we used surveillance data from the country of interest (China, Egypt, Cambodia, Indonesia, Thailand or Vietnam) to estimate country-specific relative incidence. When fewer than 50 specimens were reported for a given country in a given year, we substituted surveillance data from the same year, across all other countries of interest with adequate data. For years in which no surveillance data was available from any H5N1 or H7N9 affected country (1977-1996), we substituted surveillance data from laboratories in the United States *(47)*. From 1997-2015, the relative incidence of H3N2 or H1N1 in the United States was significantly correlated with subtype-specific relative incidence in our study's six countries of interest (Pearson's $r = 0.70$, $p < 0.001$), suggesting that US data is a reasonable proxy.

A priori predictions

The *a priori* predictions in Fig. 2 illustrate how the observed total number of cases would be distributed across birth years if individuals with protective HA imprinting never experienced severe infection, but risk is otherwise identical for everyone. Thus, the distribution of observed cases across birth years was expected to be proportional to the distribution of unprotected individuals across birth years (i.e. to the demographic age

distribution, after individuals with protective HA imprinting had been removed). For each country and year in which cases were observed, this *a priori* prediction is:

$$P_{yci} = \frac{D_{yci} w_{o,i|y,c}}{\sum_i D_{yci} w_{o,i|y,c}} \quad (8)$$

Here, P_{yci} is the fraction of all cases observed in country c, year y predicted to occur in birth year i. D_{yci} represents the demographic age distribution as defined in equation 1. Building from equations 6 and 7, $w_{o,i|y,c}$ represents the fraction of each birth cohort with first exposure to a subtype in the opposite HA group as the challenge strain, or naïve to IAV. For the predictions shown in Figs. 2A and B, we scaled P_{yci} by the number of cases, $I_{Total,yc}$ observed in year y, country c, and then summed across all affected countries and years: $\sum_y \sum_c \left[I_{Total,yc} P_{yci} \right]$. For the predictions shown in Figs. 2C and D, we subtracted the demographic null expectation (as in equations 1 and 2), to obtain the prediction: $\sum_y \sum_c \left[(I_{Total,yc} P_{yci}) - Exp_{yci} \right]$.

Sensitivity analyses

We verified that our conclusions are robust to model assumptions by repeating model fitting and model comparison on twelve variations of the main model described above (Fig. S7). First, to test for robustness against uncertainty on annual intensity of seasonal IAV circulation, we repeated all model analyses assuming a constant annual attack rate ($a_j = a$ for all years j). Second and third, we considered uncertainty on the baseline attack rate, a, by setting this parameter equal to its upper and lower 95% confidence bounds. Fourth, we checked for robustness to the estimated annual dominance of H1N1 and H3N2 by fixing the relative incidence of each to its average from 1977 to 2015 (0.34 for H1N1, 0.66 for H3N2). Fifth and sixth, to generate upper and lower bound estimates of either subtype's seasonal dominance, we increased the observed relative incidence of H1N1 or H3N2 by 0.05 for all years from 1977-2015, while simultaneously decreasing the relative incidence of the complementary subtype by the same amount. Seventh and eighth, we considered two alternate poultry-risk distributions, using data exclusively from Urban Shenzhen *(6)* and Shanghai *(7)* as data from these surveys respectively reported the highest and lowest poultry exposure rates in cohorts born before 1968. Ninth through eleventh, although overall influenza vaccine coverage is low in all six countries considered (approaching 10% in Thailand and <5% elsewhere) *(48)*, we tested whether our analysis is robust to childhood vaccination effects. We considered three scenarios, in which vaccination of naïve children could prevent imprinting and leave the child fully susceptible to both HA groups, replace imprinting and leave the child protected against both HA groups or delay imprinting via delay of the first natural infection. To be conservative, these models considered an upper-bound case for IAV vaccination coverage, and assumed childhood coverage levels beyond what is actually achieved in H5N1- and H7N9-affected countries (Supplementary Text). Finally, to verify that our results were robust to the exclusion of data from probable or suspected cases, we repeated model analyses using only laboratory-confirmed cases.

Phylogenetic and amino acid sequence analyses

We aligned amino acid sequences of representative H1 strains (HA globular head) and group 1 and group 2 HA strains (stem domain) in Geneious v9.0.4 *(49)* (global alignment with free end gaps, BLOSUM62 cost matrix). Maximum likelihood phylogenies were estimated in RAxML version 7.2.8 *(50)* using the aligned amino acid sequences and a GAMMA LG protein model (rapid hill-climbing algorithm). We generated a heat map of HA stem amino acid sequences with percent similarities (BLOSUM62 matrix with threshold 0) calculated in Geneious version 9.0.4 *(49)*.

Projections of future pandemics

We used a discrete-time stochastic model to create projections of the age-specific severe attack rates in a hypothetical future H7 or H5 pandemic. We conducted simulations for the United Kingdom, China, and Vietnam in 2015 and 2025. For the 2025 simulations, we considered two scenarios for seasonal IAV circulation between 2015 and 2025: 25% group 1 and 75% group 1 circulation. Demography and imprinting patterns for each country and year were obtained as described in Methods (see 'Normalization to demographic data' and 'Reconstructing immune imprinting patterns').

In the model, individuals with matched imprinting have probability $(1 - H_m)$ of experiencing a 'protected' course of infection and a probability H_m of experiencing the same 'unprotected' infection as individuals with mismatched imprinting. 'Protected' individuals have some degree of acquired immune protection and do not experience severe disease; to be conservative, we assume that they still become infected but their lower viral loads lead to reduced infectiousness relative to their 'unprotected' counterparts (mediated by a relative infectiousness parameter, α). As discussed in the main text, this assumption mirrors data from experimental infections in humans and non-human animals, which show that infections in partially-protected individuals exhibit lower viral titers, lower and more short-lived viral shedding, and lower rates of transmission than infections in naïve individuals *(22, 24, 25)*. In our analyses, we tested values of α spanning from 0.1 to 0.9, representing the full range of possible reductions in transmission. We expect that the true value for a given situation would depend on specific properties of the focal IAV strain as well as the past strains that generated the imprinted responses.

An 'unprotected' infected individual in age group i exposes a total of X_{ij} individuals from age group j to the virus, where X_{ij} follows a negative binomial distribution with dispersion parameter $k = 0.94$ *(51)* and mean M_{ij}. For 'protected' infected individuals, the mean number of new infections is instead αM_{ij}. The matrix **M** (with entries M_{ij}) is the next generation matrix with dominant eigenvalue equal to the pathogen's basic reproductive number (R_0). R_0 was set at 2.5 so that the effective reproductive number (R_{eff}), which accounts for protection from matched imprinting, was approximately 1.9 at the beginning of the 2015 simulations. This value aligns with the R_{eff} calculated at the beginning of previous pandemics *(52-56)*.

An unscaled next generation matrix **M** was constructed from data on contact rates between age groups. Separate contact matrices giving the relative rates of contacts between individuals in different age groups were used for each country. For the UK, we used the matrix of all reported physical and non-physical contacts in Great Britain

reported by Mossong et al. *(30)*; for China, we used data on individual-level contacts reported by Read et al. *(31)*; and for Vietnam, we used contact diary data from Horby et al. (individual-level data provided by Peter Horby) *(32)*. We converted the China and Vietnam contact data from the reported age bins into the age bins needed for simulations by disaggregating the reported data (scaled by demography) into separate age years and then reaggregating the data into the appropriate age bins. All elements of this matrix were rescaled by a constant factor so that its dominant eigenvalue was equal to the desired R_0.

The X_{ij} exposures caused by an infectious individual were assumed to occur after a serial interval of T days from the source case, where T was distributed according to a Weibull distribution with mean 3.6 (shape = 2.3 and scale = 4.1) *(57)*. Given exposure on day t, the probability that an individual in age group j developed the disease was equal to the proportion of age group j susceptible on day t.

Each individual that experienced an 'unprotected' course of infection had a chance of developing a severe infection. The probability of severe infection is a property of a given viral strain (roughly, its virulence) and will vary among scenarios; we chose a baseline value of 0.1, and note that different choices for this value simply rescale the results and do not alter any qualitative patterns. To account for the elevated risk of severe infection in children (0-4 years) and the elderly (65+), the probability of severe infection in these age groups was multiplied by the age-specific risk parameters A_c and A_e. We used consensus parameter estimates for A_c and A_e, which should most robustly represent the behavior of pandemic strains that cause large numbers of cases in both old and young age groups. To obtain these values, we set H_m at 0.245 (the midpoint value from our main analyses; see Table 1), constrained A_c and A_e to be identical for H5N1 and H7N9, and estimated the parameter values by maximizing the constrained likelihood.

We used three sets of assumptions to explore how vaccination of naïve children might affect imprinting for the 2015 UK simulation. In the first set, we assumed that vaccination had no impact on imprinting patterns in the population (this assumption is used in the simulations for all other years and countries). In the second set, we assumed that children who were vaccinated against seasonal influenza before experiencing their first natural IAV infection obtained full imprinting protection against both HA group 1 and 2 IAVs. In the third set, we assumed that children who were vaccinated before experiencing their first natural IAV infection were blocked from imprinting on either HA group and experienced no imprinting protection.

Seasonal influenza vaccination was first recommended in the UK for individuals in certain high risk groups in the late 1960s *(58)*. Before 2013, influenza vaccination was only recommended for children in certain clinical risk groups, and vaccine coverage across all children was rarely measured. Beginning in 2013, the UK began a phased introduction of influenza vaccination in children, and regular surveys measuring the vaccine coverage rates became available *(59, 60)*. For the model, we assumed a linear rate of increase between 1966 and 2012, assuming 0% coverage in 1966 and using the estimated 13.4% coverage of children aged 0-2 in 2007 to calibrate the rate of coverage increase between 1966 and 2012 *(61)*. For 2013, 2014, and 2015, the maximal coverage values reported in age groups 0-5 were used: these were 42.6%, 41.3%, and 54.4%, respectively *(60, 62)*.

One hundred simulations were run for each pandemic scenario. To appropriately represent all sources of uncertainty, each simulation was run with independent values of H_m, A_c, and A_e drawn from the relevant sampling distributions.

Projections of R_{eff} (Fig. 3B, Fig. S9) were created for the UK, China, and Vietnam, assuming that a group 1 HA had constant seasonal dominance of 0%, 25%, 75%, or 100% from 2015 to 2060. For a given country, seasonal dominance scenario, and year, the fraction of each birth-year cohort with first exposure to each HA group was calculated as described in Methods (Reconstructing immune imprinting patterns) and used in conjunction with H_m to calculate the proportion of each birth-year cohort that would experience a 'protected' versus 'unprotected' course of infection with H5 or H7 IAV. The next generation matrix for a fully naïve population **M** (described in the previous section) was modified to separate 'protected' and 'unprotected' individuals, and account for the reduced infectiousness of 'protected' individuals (governed by α), and R_{eff} was calculated as the dominant eigenvalue of this matrix.

Supplementary Text

Contents:

1. Likelihood Functions

The probability density function for the multinomial distribution is:

$$P(x_1, x_2, \ldots x_n) = \frac{n!}{\prod x_i!} \prod {p_i}^{x_i} \quad \text{(S1)}$$

In our analysis, for a given country in a given year, we considered the multinomial probability of observing a certain number of cases or fatalities, x_i, in each birth year, i. Each of our models assumes different factors may influence p_i, the probability that any case has birth year i.

To find the likelihood of the full data, which comes from several countries in several case observation years, we multiply the multinomial probabilities from all relevant countries, c, and all relevant years of case observation, y. The full likelihood is:

$$L = \prod_y \prod_C \left[\frac{n_{yc}!}{\prod x_{yci}!} \prod p_{yci}^{x_{yci}} \right] \quad \text{(S2)}$$

From equation S2, we obtain the full log likelihood:

$$L = \sum_y \sum_c \left[\log(n_{yc}!) - \sum_i \log(x_{yci}!) + \sum_i x_{yci} \log(p_{yci}) \right] \quad \text{(S3)}$$

Maximum likelihood estimation was performed in R (version 3.2.0) and the optim() function was used to minimize the negative log likelihoods of candidate models. Code for model fitting is provided as a supplementary data file.

2. Model equations

Each model below assumes that a unique combination of five possible factors determine p_{yci}, the probability that an infection or death observed in year *y,* country *c*, occurred in birth cohort *i* (Methods, Table S1). Demography (D) serves as the null hypothesis for the distribution of cases across birth years, and appears in every model. We assume all additional factors act independently. In all models, we normalize the probabilities to ensure $\sum_{i=1918}^{y} p_{yci} = 1$.

2.1 Demography (D)

This model assumes incidence in each birth year should be proportional to the fraction of the population of country *c*, year *y*, born in the year of interest.

$$p_{yci} = D_{yci} \quad \text{(S4)}$$

D_{yci} = Fraction born in year *i*, of the total population of country *c* born between 1918 and the case observation year (*y*).

2.2 Demography + exposure (DE)

This model adds a factor describing poultry exposure risk across age groups.

$$p_{yci} = D_{yci} E_{yi} \quad \text{(S5)}$$

E_{yi} = Proportional risk in each birth year cohort, based on the frequency with which individuals of a given age (birth year *i*, in year *y*) contact poultry.

2.3 Demography + age-based risk (DA)

This model introduces parameters that allow children ages 0-4 or the elderly ages 65+ to experience increased risk relative to other children and adults.

$$p_{yci} = D_{yci}(u_{c_{yi}} A_c + u_{e_{yi}} A_e + u_{a_{yi}}) \quad \text{(S6)}$$

Group indicators

- $u_{c_{yi}}$ = Indicator of membership in the age group representing high-risk children, taking value 1 for birth year cohorts of age 0-4 in year *y*, and 0 for all others.
- $u_{a_{yi}}$ = Indicator of membership in the reference age group, taking value 1 for birth year cohorts of age 5-64 in year *y*, and 0 for all others.
- $u_{e_{yi}}$ = Indicator of membership in the high-risk, elderly age group, taking value 1 for birth year cohorts of age 65+ in year *y*, and 0 for all others.

Parameters

- A_c = Proportional increase in risk for children ages 0-4, relative to the reference age group.
- A_e = Proportional increase in risk for the elderly, ages 65+, relative to the reference age group.

2.4 Demography + hemagglutinin imprinting (DH)

This model introduces parameter H_m, which allows individuals with group-matched first hemagglutinin exposures to experience decreased risk relative to all others.

$$p_{yci} = D_{yci}(w_{m,i|y,c}\, H_m + w_{o,i|y,c}) \quad \text{(S7)}$$

Group indicators

- $w_{m,i|y,c}$= Faction of each birth cohort with protective HA imprinting (group-matched to the challenge strain). This group should experience reduced risk under the HA imprinting hypothesis.
- $w_{o,i|y,c}$ = Fraction of each birth cohort without protective HA imprinting. This group includes both IAV-naïve children and all individuals with HA-mismatched first exposures.

Parameters

- H_m = Proportional risk for individuals with group-matched first hemagglutinin exposures, relative to all others. H_m takes values in the range [0, 1], where 0 indicates full protection and 1 indicates no additional protection relative to the reference group.

2.5 Demography + neuraminidase imprinting (DN)

This model introduces parameter N_m, which, similarly to the DH model above, allows those with group-matched first neuraminidase exposures to experience decreased risk.

$$p_{yci} = D_{yci}(w_{m,i|y,c}N_m + w_{o,i|y,c}) \quad \text{(S8)}$$

Group indicators

- $w_{m,i|y,c}$= Fraction of each birth cohort with NA imprinting group-matched to the challenge strain.
- $w_{o,i|y,c}$ = Fraction of each birth cohort without protective NA imprinting.

Parameters

- N_m = proportional reduction in risk for individuals with group-matched first hemagglutinin exposures, relative to all others. N_m takes values in the range [0, 1], where 0 indicates full protection and 1 indicates no additional protection relative to the reference group.

2.6 Demography + neuraminidase imprinting + hemagglutinin imprinting (DNH)
This model includes protection from first exposure to a group-matched HA (as in the DH model) as well as a group-matched NA (as in the DN model).

$$p_{yci} = D_{yci}(H_m N_m w_{mm,i|y,c} + H_m w_{mo,i|y,c} + N_m w_{om,i|y,c} + w_{oo,i|y,c}) \quad \text{(S9)}$$

Group indicators

- $w_{mm,i|y,c}$ = Fraction of each birth cohort with matched imprinting to HA and NA.
- $w_{mo,i|y,c}$ = Fraction of each birth cohort with matched HA imprinting and mismatched NA imprinting.
- $w_{om,i|y,c}$ = Fraction of each birth cohort with mismatched HA imprinting and matched NA imprinting.
- $w_{oo,i|y,c}$ = Fraction of each birth cohort with mismatched imprinting to HA and NA, or that is naïve to IAV infection.

2.7 Demography + age-based risk + hemagglutinin imprinting (DAH)
This model assumes that demography, age-based risk and HA imprinting determine overall risk.

$$p_{yci} = D_{yci}(w_{m,i|y,c} H_m + w_{o,i|y,c})(u_{c_{yi}} A_c + u_{e_{yi}} A_e + u_{a_{yi}}) \quad \text{(S10)}$$

2.8 Demography + age-based risk + neuraminidase imprinting (DAN)
This model assumes that demography, age-based risk and neuraminidase imprinting, determine overall risk.

$$p_{yci} = D_{yci}(w_{m,i|y,c} N_m + w_{o,i|y,c})(u_{c_{yi}} A_c + u_{e_{yi}} A_e + u_{a_{yi}}) \quad \text{(S11)}$$

2.9 Demography + age-based risk + neuraminidase imprinting + hemagglutinin imprinting (DANH)
This model assumes that demography, age-based risk, neuraminidase imprinting and hemagglutinin imprinting determine overall risk.

$$p_{yci} = D_{yci}\left(H_m N_m w_{mm,i|y,c} + H_m w_{mo,i|y,c} + N_m w_{om,i|y,c} + w_{oo,i|y,c}\right)(u_{c_{yi}} A_c + u_{e_{yi}} A_e + u_{a_{yi}}) \quad \text{(S12)}$$

2.10 Demography + exposure + age-based risk (DEA)
This model assumes that demography, exposure frequency and age-based risk determine overall risk.

$$p_{yci} = D_{yci}E_{yi}(u_{c_{yi}}A_c + u_{e_{yi}}A_e + u_{a_{yi}}) \quad \text{(S13)}$$

2.11 Demography + exposure + hemagglutinin imprinting (DEH)
This model assumes that demography, exposure frequency and hemagglutinin history determine overall risk.

$$p_{yci} = D_{yci}E_{yi}(w_{m,i|y,c}H_m + w_{o,i|y,c}) \quad \text{(S14)}$$

2.12 Demography + exposure + neuraminidase imprinting (DEN)
This model assumes that demography, exposure frequency and neuraminidase history determine overall risk.

$$p_{yci} = D_{yci}E_{yi}(w_{m,i|y,c}N_m + w_{o,i|y,c}) \quad \text{(S15)}$$

2.13 Demography + exposure + age-based risk + hemagglutinin imprinting (DEAH)
This model assumes that demography, exposure frequency, age-based risk and hemagglutinin imprinting determine overall risk.

$$p_{yci} = D_{yci}E_{yi}(w_{m,i|y,c}H_m + w_{o,i|y,c})(u_{c_{yi}}A_c + u_{e_{yi}}A_e + u_{a_{yi}}) \quad \text{(S16)}$$

2.14 Demography + exposure + age-based risk + neuraminidase imprinting (DEAN)
This model assumes that demography, exposure frequency, age-based risk and neuraminidase imprinting determine overall risk.

$$p_{yci} = D_{yci}E_{yi}\left(w_{m,i|y,c}N_m + w_{o,i|y,c}\right)\left(u_{c_{yi}}A_c + u_{e_{yi}}A_e + u_{a_{yi}}\right) \quad \text{(S17)}$$

2.15 Demography + exposure + neuraminidase imprinting + hemagglutinin imprinting (DENH)
This model assumes that demography, exposure frequency, hemagglutinin imprinting and neuraminidase imprinting determine overall risk.

$$p_{yci} = D_{yci}E_{yi}(H_mN_mw_{mm,i|y,c} + H_mw_{mo,i|y,c} + N_mw_{om,i|y,c} + w_{oo,i|y,c}) \quad \text{(S18)}$$

2.16 Demography + exposure + age-based risk + neuraminidase imprinting + hemagglutinin imprinting (DEANH)

This model assumes that demography, exposure frequency, age-based risk, neuraminidase imprinting and hemagglutinin imprinting determine overall risk.

$$p_{yci} = D_{yci}E_{yi}(H_m N_m w_{mm,i|y,c} + H_m w_{mo,i|y,c} + N_m w_{om,i|y,c} + w_{oo,i|y,c})(u_{c_{yi}}A_c + u_{e_{yi}}A_e + u_{a_{yi}}) \quad \text{(S19)}$$

3. Reconstructing HA imprinting patterns with vaccination

When IAV-naïve children receive the seasonal influenza vaccine, the effect on HA imprinting in these children is unknown. We chose not to consider childhood vaccination in our main analysis, but instead to consider its possible effects via subsequent sensitivity analyses. Our rationale for omitting childhood vaccination in our main analysis was based on three main arguments.

First, childhood vaccination coverage is low in all H5N1- and H7N9-affected countries, so any effects of childhood vaccination on our results would be small. China and Thailand have recently launched public health initiatives to encourage early childhood influenza vaccination. However, even in these countries, recent estimates of childhood vaccine coverage are relatively low (and quite variable), ranging from 1% *(63)* to 30% *(64)* in Thailand, and from 26% *(65)* in China to <9% *(66)* in Hong Kong. For all other countries in our study, conservative estimates based on the number of vaccine doses purchased *(48)* show that even in the upper-bound limit that all vaccine doses were administered, and were distributed exclusively among children ages 0-9 years, childhood coverage would remain well below 5% in these countries (details below).

Second, early childhood influenza vaccination has only been widely recommended since the mid-late 2000's *(64, 67)*. Thus, the great majority of birth cohorts in our study would not have been affected at all. Since our study's conclusions are driven most strongly by the dramatic change from group 1 to group 2 HA imprinting around the 1968 birth year, our conclusions are robust to variation in HA imprinting patterns in the very young birth cohorts that could have been affected by very recent, moderate increases in early childhood vaccination.

Third, for naïve children, single-dose influenza vaccine efficacy is exceptionally low, so the coverage estimates stated above strongly overestimate the effective vaccine coverage levels relevant to our analysis. IAV-naïve individuals require a series of two vaccine doses for effective protection *(67, 68)*. However, in the United States, CDC data shows that only about 60% of children aged 6-24 months complete the two-dose course. We have not found equivalent data for H5N1- or H7N9-affected countries, but two-dose compliance is unlikely to be drastically better than in the US.

Given these arguments, we expected that childhood vaccination would have a minimal impact on our main findings, no matter how vaccination of IAV-naïve children affects HA imprinting at the individual scale. To test this expectation, we performed sensitivity analyses that considered three possible effects of imprinting: 1, vaccination of naïve children could prevent imprinting to either HA group, 2, vaccination of naïve

children could cause dual imprinting to both HA groups or 3, vaccination of naïve children could delay the first natural infection and hence delay imprinting.

All of these sensitivity analyses required estimates of childhood vaccination coverage and efficacy for each country and year. Because reported estimates of childhood vaccine coverage vary considerably among studies, we estimated conservative, upper-bound limits on the true coverage to test the maximum effect childhood vaccination might have on our findings. We used data from Palache et al. *(48)* to determine the total number of vaccine doses distributed in each country of interest over time. For each year, we made the conservative assumption that all doses within the country were administered, and distributed uniformly among children ages 0-9. In reality, not all doses are administered, and administered doses are actually distributed across all age groups, not exclusively in young children. Furthermore, while some naïve children would in reality receive two vaccine doses, we estimated upper-bound coverage levels as though all children required only one dose. We assumed vaccine efficacy was 60% in all non-pandemic years. This upper-bound efficacy estimate reflects that, as discussed above, at most 60% of naïve children complete the required two-dose course *(67)*. This efficacy estimate is further conservative because even among children that receive two doses, the vaccine will not be perfectly protective due to antigenic drift.

In our first sensitivity analysis, we assumed that vaccination of IAV-naïve children delays the first natural infection, and hence delays imprinting, but does not affect imprinting otherwise. To estimate the fraction of each birth cohort with imprinting to particular seasonal subtypes, we incorporated the assumed vaccine-induced delay of imprinting by revising the definition of the annual attack rate on children, a_j (see equation 4 in Methods):

$$a_j' = \left(1 - v_j e_j\right) a I_j \tag{S20}$$

Here v_j describes childhood IAV coverage in year j, e_j describes IAV vaccine efficacy, a represents the baseline attack rate on children and I_j represents the year's intensity score. With these modifications, we estimated vaccine-influenced imprinting patterns and performed model analyses as described in the Methods (Reconstructing immune imprinting patterns).

In our second and third sensitivity analyses, we assumed vaccination would prevent or replace imprinting in IAV-naïve children, so all children vaccinated before their first natural infection would either remain fully susceptible to both HA groups, or would simultaneously imprint to both groups. Here, it became necessary to keep track of the fraction first exposed via natural infection, the fraction first exposed via vaccination, and the fraction that remained naïve in the first 12 years after the birth year. We computed these using a recursive approach:

$$\varepsilon_{ij}' = n_{i,j-1}\left(1 - v_i e_j\right) a I_j \tag{S21}$$

$$\lambda_{ij} = n_{i,j-1}\, v_i e_j \tag{S22}$$

$$n_{ij} = n_{i,j-1}\,(1 - v_i e_j)(1 - a I_j) \tag{S23}$$

Here, as in equation 3 and 4, ε_{ij}' represents the fraction of birth cohort *i* that was first naturally infected in year *j* (prime indicates modification of the main text definition). λ_{ij} represents the fraction of birth cohort *i* that was first vaccinated (prior to their first natural exposure) in year *j*. n_{ij} represents the fraction of cohort *i* that remained naïve at the beginning of year *j,* and was thus eligible for first infection or vaccination as year *j* progressed. In the first year of life (when *j* = *i*), n_{ii} is set to 1, indicating that all newborns are initially naïve. In all subsequent years, *j,* probabilities of first vaccination or natural infection were only applied to the naïve fraction of the cohort. Parameters v_j, e_j, a and I_j are as defined above.

After calculating relevant raw values of ε_{ij}' and λ_{ij}, we applied a normalizing factor, $N_{i|y}'$ to all ε_{ij}' and $\lambda_{ij.}$ As discussed in equation 4, the normalizing factor reflects the assumption that all individuals have their first natural infection or vaccination by age 12, and ensures that all relevant probabilities for a birth year sum to 1. It is given by:

$$N_{i|y}' = \begin{Bmatrix} \sum_{j=i}^{i+12}(\varepsilon_{ij} + \lambda_{ij}) & y \geq i+12 \\ 1 & y < i+12 \end{Bmatrix} \quad \text{(S24)}$$

Finally, in the analysis assuming that vaccination of IAV-naïve children prevents imprinting, we always assigned the fraction of each cohort that was vaccinated before the first natural infection, $\sum_j \lambda_{ij,}$ to the mismatched-imprinting group, $w_{o,i|y,c}$, as defined in equation 6 above. In the analysis assuming that vaccination of IAV-naïve children causes dual imprinting, we always assigned fraction $\sum_j \lambda_{ij}$ to the matched-imprinting group, $w_{m,i|y,c}$. Even at the upper limits of plausible vaccination coverage rates, our main results remained robust in all three sensitivity analyses (Fig. S7).

4. Annual intensity of influenza circulation from 1918-2015

Before 1977, the annual intensity of influenza circulation (which scales the annual attack rate) has minimal influence on imprinting patterns, since the dominant HA group changed only once, during the 1968 pandemic. To model the post-1977 era of H3N2 and H1N1 co-circulation, when the dominant HA group could change on yearly rather than pandemic timescales, we obtained virological surveillance data from WHO collaborating laboratories. These data are available from 1977-2015, providing a direct measure of annual IAV incidence. In years prior to 1977, the best estimates of the annual influenza burden come from pneumonia and influenza (P&I) excess mortality data from the United States *(69)*. Thus, to estimate annual IAV intensity, we compiled estimates of incidence from virological surveillance data in years 1977-2015, and P&I excess mortality data in years 1918-1976. Sensitivity analyses (Fig. S7) confirmed that our study's results are quantitatively and qualitatively robust to uncertainty in the intensity index, and the results also remained robust when we replaced the intensity index with a constant value.

For 1997-2015 we obtained influenza surveillance data from our study's six countries of interest. To shield against local biases in case ascertainment and small sample sizes, we aggregated data across all six countries to model annual intensity. We defined raw annual incidence as: $\frac{Total\ IAV\ positive\ specimens\ in\ all\ countries}{Total\ IAV\ specimens\ processed\ in\ all\ countries}$. In years when the total number of reported specimens processed across all six affected countries was

less than 50 (1997, 2000 and 2001), we substituted surveillance data from the United States. For 1977-1996 we could not find influenza surveillance data from countries affected by H5N1 and H7N9. Thus, we also substituted data from the United States for this time period *(47)*.

After aggregating influenza surveillance data for all years from 1977-2015, we found that the observed annual incidence of influenza has increased predictably over time. A linear regression showed that the proportion of positive IAV specimens increased by about 0.0019/year (SE = 0.0006, p = 0.005). We assume this trend reflects a steady improvement in case detection efficiency, perhaps due to improved diagnostics or more targeted sampling, rather than a true increase in the annual influenza incidence proportion. Thus, we used this linear model to define yearly, expected incidence values for 1977-2015, and then defined annual circulation intensity as the ratio of observed to expected incidence.

For 1918-1976, we compiled published estimates of pneumonia and influenza (P&I) excess mortality rates, per 100,000 population, for each year *(69-74)*. Because northern hemisphere influenza seasons occur in the winter, estimates were not always reported on a calendar year basis. Instead, rates were often reported for a defined outbreak period, beginning and ending in specified months. In these cases, to adjust to the calendar year basis on which we defined birth cohorts, we first determined the fraction of outbreak months occurring within each calendar year, and then allocated the appropriate fraction of the season's total excess mortality to either relevant year. By definition, excess mortality takes only non-negative values, but intensity values informed by surveillance data could be positive or negative (Fig. S10 A). To verify that our results are robust to this discrepancy, we performed a sensitivity analysis in which we shifted all P&I scores down by their mean (thus allowing the P&I series to also take positive and negative values). This did not change the results of model selection, or notably change the maximum likelihood value of parameter H_m. Because we used our intensity time series to inform IAV imprinting patterns, we set excess mortality equal to zero in years dominated by type B influenza. In years when types A and B were co-dominant, we attributed half the total reported excess mortality to influenza A.

When verifying the comparability of excess mortality and incidence data, we found that the variance in post-1977 intensity estimates (informed by virological surveillance data) was greater than the variance in 1918-1976 estimates (informed by excess mortality data). To correct this discrepancy, we scaled the variance in the older P&I data set to match the variance of non-negative values in more recent surveillance-based estimates (thus giving the two series similar amplitude). We allowed a maximum intensity score of 2.5, to maintain a reasonable maximum annual attack rate of 0.75 or less. The maximum score applied only in years 1918, 1919, 1944 and 2009, all of which are recognized as years of intense influenza circulation. Annual intensity values and corresponding attack rates are shown in Fig. S10.

5. Country-specific model fits and model selection

We conducted the full maximum likelihood estimation and model comparison analysis for each of the six countries in our study, in isolation. We found that strong support for HA imprinting effects was maintained in these country-specific analyses. In

the four countries with the most cases (China, Egypt, Indonesia and Vietnam, $n \geq 75$), the best models all included HA imprinting, with estimates of protective efficacy (H_m) very similar to the estimate in the main text. In Thailand ($n = 28$), and Cambodia ($n = 57$), despite very low numbers of cases, models including HA imprinting effects were the second most preferred in model selection, and were statistically indistinguishable from the best models, with ΔAIC of 0.45 and 0.47, respectively. Country-specific case distributions, model fits and the results of country-specific model comparison are shown in Fig. S11.

These analyses show that patterns in all countries are qualitatively consistent with core findings presented in the main text: in each of the countries, very few H5N1 cases are observed in cohorts born before 1968. The major distinction among countries is the difference in number of H5N1 cases reported in children (i.e. birth-years since 2005). Relative to the consensus model, excess cases are observed in children in Cambodia and Egypt, but a shortfall of cases in children is observed in Indonesia, China and Vietnam. Country-specific variation in poultry contact, access to healthcare, or case reporting for children could explain these differences. Variation in imprinting patterns (resulting from different experiences with the 2009 pandemic in different regions) could also be at play. While we do not have data to test these potential explanations, we note that children are not under-represented for H7N9 in China (the one country where we can make a direct comparison), which weighs against the former explanations in this one country at least.

6. Cross-validation analysis

To verify that our data sets are large enough to produce robust model comparison results, and to assess the out-of-sample predictive capability of our models, we performed two-fold cross-validation. We performed these analyses for H5N1 and H7N9 data. Each trial consisted of the following steps:

i. Randomly partition the data set (of H5N1 or H7N9 cases) into two equal subsets. Designate one half of the data as the training set, and the other half as the test set.
ii. Fit all 16 models (D, DR, DH, DN, …etc.) to the training set, determining maximum-likelihood estimates of all model parameters. Calculate AIC values to determine which fitted model performs best on the training set.
iii. Find the likelihood of the test data, given all models and their maximum-likelihood parameter estimates (determined in step ii, using the training set). Determine which model is the best fit to the test data based on likelihood.
iv. Test for robustness to reduced sample size: Are HA imprinting effects included in the best model from step ii, after fitting to a data set of half the size used in the main text analysis? Does the best model match the preferred model from the main text?
v. Test the best model's performance on out-of-sample data: Does the best model for the test data contain HA imprinting effects? Does it match the preferred model from the main text?
vi. Now, switch the subset assignments, so the original test set becomes the new training set, and vice versa. Repeat steps ii-v.

We performed 100 cross-validation trials for each of the H5N1 and H7N9 data sets (so 200 unique training sets were used, see step vi). For H5N1, DRH (the preferred model in the main text analysis) remained the best model for 99% of the training sets. The median and central 95% of H_m estimates were 0.25 (0.17-0.32). For H7N9, DERH (the preferred model in the main text analysis) remained the best model for 100% of the training sets. The median and central 95% of H_m estimates were 0.24 (0.17-0.33). For both H5N1 and H7N9, these H_m values are statistically indistinguishable from estimates obtained using the full data set (see Table S2). Thus, for both H5N1 and H7N9, our core results are robust to the exclusion of half of our available data.

These same models were also strongly preferred by the test sets—DRH was the best model for 92% of H5N1 test sets and DERH was the best model for 97.5% of H7N9 test sets. In all cases, the best model for the test set included HA imprinting effects. Thus, barring major changes to the biology or epidemiology of these viruses, the best models presented in the main text are suitable for approximate prediction of the birth year distributions of newly arising cases, and HA imprinting effects remain an important predictor in all cases.

7. Robustness to age biases in case ascertainment

Epidemiological data sets are always subject to possible biases in case ascertainment. As discussed above, we introduced age-based risk parameters A_c and A_e to allow for the increased risk of severe infection (and associated increase in case ascertainment) for children and the elderly, a known pattern from seasonal influenza epidemiology *(41)*. However, other forms of age-specific bias might be present in the data sets we analyzed. Given the centrality of age-related patterns to our findings (insofar as they are connected to birth year), we undertook an extreme test of whether our core results are robust to a hypothetical worst-case bias in case ascertainment. Specifically, we tested the effect of a hypothetical bias that systematically degraded the strongest signal of HA imprinting in the data, i.e. the 1968 shift from group 1 to group 2 dominance in seasonal IAV strains. Thus we used simulations to consider scenarios in which severe H5N1 cases born before 1968, or severe H7N9 cases born after 1968, had lower probabilities of being ascertained, relative to cases in other birth years.

We note that this is a 'perfectly bad' reporting bias, and is based on birth year rather than age (and hence would require the bias to drift systematically over nearly two decades, for H5N1). Also, we emphasize that our work focuses on the influence of imprinting on severe cases of disease, which are much less likely to be subject to reporting bias than mild or subclinical cases. A recent review of H5N1 and H7N9 epidemiology by Qin et al *(1)* did highlight the potential for under-ascertainment of milder cases of H7N9, which are disproportionately found in younger individuals (and are often found in the course of cluster investigations, following severe index cases). Crucially, this is exactly the pattern that our findings would predict, since younger individuals are more likely to be imprinted on group 2 HA and hence protected from severe H7 disease. Qin et al. did not find any evidence of substantial under-ascertainment of H5N1 cases, and do not suggest any age bias in reporting.

For H5N1, we considered scenarios where severe cases occurring in older, pre-1968 birth cohorts were 50%, 33% or 25% as likely to be observed as cases in younger,

post-1968 cohorts. Thus, we used simulation to add hypothetical unobserved cases into the data set, increasing the number of H5N1 cases by a factor of 2, 3 or 4 in the pre-1968 cohorts where these cases are rare in the real data. Effectively, this decreased differences in apparent risk between pre- and post-1968 birth cohorts, systematically diminishing the signature of HA imprinting effects.

Similarly, for H7N9, we considered scenarios where severe cases occurring in underrepresented, post-1968 birth cohorts were 50%, 33% or 25% as likely to be observed as cases occurring in older cohorts. We again used simulation to increase the number of cases in underrepresented cohorts by factors of 2, 3 or 4, respectively.

The number of cases added to each country-year depended on the number of cases observed in the same country-year in underrepresented cohorts for H5N1 (1918-1968), or H7N9 (1969-2015). This number was multiplied by the factor required to double, triple or quadruple the number of cases in these augmented birth cohorts. The probability that an added case was assigned to a particular birth year was proportional to the demographic age distribution across augmented birth years for the country and year of interest. For each virus and assumed relative detection probability, we generated 100 augmented data sets. We performed model fitting and comparison on each augmented data set to determine whether HA imprinting would remain a factor in the best model, and to quantify the value of parameter H_m in these best models. Representative trials are shown in Fig. S12.

We found that both H5N1 and H7N9 were robust to 'perfectly bad' age-biased reporting at the 50% reporting level: the DAH model remained the selected model in all 100 trials for H5N1, with a median H_m parameter estimate of 0.54; similarly, the DEAH model remained the selected model in all 100 trials for H7N9, with a median H_m parameter estimate of 0.54. For H7N9, even larger, 'perfectly bad' biases did not change the core finding. At the 33% and 25% levels, model selection still supported HA imprinting in 99% and 85% of trials, respectively (though the preferred model switched from DEAH to DAH). For H5N1, at the 33% relative detection level, DRH remained the best model in 76% of trials (with a weak H_m parameter estimate), but in the remaining 24/100 trials, HA imprinting effects were not included in the best model. At 25% relative detection, only 16/100 best models included HA imprinting effects

In reality, it seems highly unlikely that case ascertainment would depend on birth year instead of age, that 1968 would coincidentally act as a key turning point separating some middle-aged adults from others, or that ascertainment of H5N1 and H7N9 cases would pivot in opposite directions around 1968. Furthermore, it seems unlikely that age or birth-year specific differences in detection of *severe* cases (the focus of our study) would differ by a factor of two or more. Thus, given the fact that our core results are robust to case ascertainment biases 3-fold or more, even with bias parameters specifically designed to degrade the imprinting signal, we are confident that plausible biases would not be large enough to challenge our study's core findings.

8. Binomial exact test for mortality

One-sided binomial exact tests showed that census-excess H5N1 mortality was significantly less likely to occur in cohorts born before 1968 (estimated probability = 0.06, CI=0.00-0.19, $p < 1e^{-6}$). For H7N9, census-excess mortality was significantly more probable in the same birth years (estimated probability = 0.94, CI=0.83-1.00, $p < 1e^{-7}$). As introduced in the main text, the same test revealed similar patterns for the incidence of H5N1 (estimated probability = 0.00, CI=0.00-0.08, $p < 1e^{-10}$) and H7N9 (estimated probability = 0.93, CI=0.84-1.00, $p < 1e^{-9}$).

9. Analysis of novel subtypes other than H5N1 and H7N9

We searched the literature and avian influenza reports for clinically significant human cases of zoonotic IAV (other than H5N1 and H7N9) in which the year and country of the case was known and the age of the infected individual was reported (n=28). We excluded cases where the clinical manifestation was limited to conjunctivitis.

To examine whether the data were better explained by the Demography (D) or the Demography + Hemagglutinin imprinting (DH) model (described in sections 2.1 and 2.4 above), we performed a simple-versus-simple hypothesis test using the likelihood ratio as the test statistic. The null distribution of the test statistic (the distribution of likelihood ratio values generated under the assumption that the D model is true) was approximated using 250,000 simulated data sets. The quantile score of the true data's likelihood ratio in this distribution was used to generate the p-value reported in the main text.

10. Parameter identifiability

We designed our family of multinomial models to allow for elevated risk of severe disease in young children and adults, via the parameters A_c and A_e respectively, to ensure that we accounted for all known age-related effects before testing our hypothesis of HA imprinting. However, a challenge arises in our study because there are very few H5N1 cases observed in the elderly, and few H7N9 cases observed in children (see Fig. 2A, B). Thus, we have little statistical power to discern possible age-based risk effects in those groups. As a consequence, our results show elevated risk in age groups where we do see cases (i.e. in children for H5N1, and in the elderly for H7N9), but age-specific effects are not detected in age groups where cases do not frequently occur (Table S2). This leads to an effect where the age-based risk appears to act in concert with HA imprinting. It is thus prudent to consider the possibility that the age-based risk parameters (A_c and A_e) and matched-imprinting protection parameter (H_m) are not perfectly identifiable.

We performed three analyses to verify that our central findings are not meaningfully affected by this potential issue with parameter identifiability. First, we plotted two-dimensional likelihood profiles for the parameter pairs of concern (figures not shown). These profiles show only weak positive correlations between the parameters H_m and A_c (for H5N1) and H_m and A_e (for H7N9). This indicates that identifiability is not a major concern. Second, from these profiles, we computed marginal 95% confidence intervals, and found values only slightly different from the univariate confidence intervals reported in Table 1 in the main text. For H5N1, the univariate CI on A_c was 1.83-2.57,

and the marginal CI from the bivariate analysis was 1.75-2.65. For H7N9, the univariate CI on A_e was 1.74-2.51, and the marginal CI from the bivariate analysis was 1.68-2.58. Again, the small differences between univariate confidence intervals and marginal, bivariate confidence intervals indicate that identifiability is not a major issue for these parameters.

Third, as a final check, we combined H5N1 and H7N9 data into a single model, and constrained parameters H_m, A_c and A_e to take the same values for both viruses (see details above in section 7). We then computed the maximum likelihood estimates for all three parameters, using the combined data set. The combined data set contained large numbers of cases in both old and young age groups, and gave us more power to estimate age-specific risk effects. The consensus estimates for A_c (1.78, 95% CI 1.53-2.07) and A_e (1.91, 95% CI 1.64-2.23) were statistically indistinguishable from the estimates of A_c (using H5N1 data) and A_e (using H7N9 data) presented in the main text analysis.

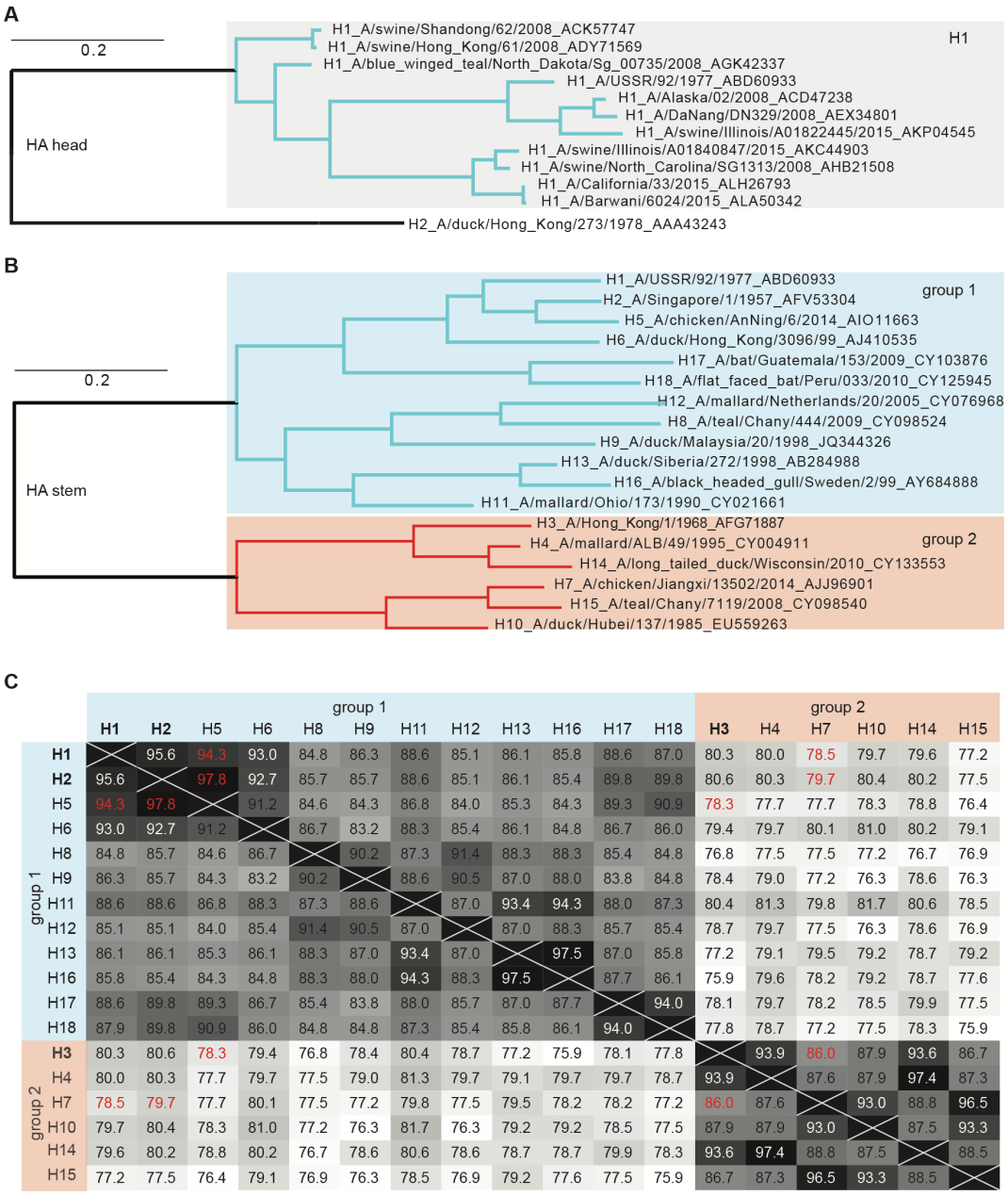

Fig. S1: Phylogenetic and sequence analyses of HA amino acids. (**A**) Maximum likelihood phylogenetic tree of H1 HA globular head amino acid sequences. (**B**) HA stem domain amino acid tree. Both trees are drawn at the same scale. (**C**) Heat map showing pairwise similarities between HA stem domain amino acid sequences (same strains as in plot **B**). The number in each cell is the percent similarity (BLOSUM62 cost matrix) for the relevant pair of sequences, with darker colors indicating higher similarity. Pairwise comparisons for H5 and H7 versus H1, H2, and H3 (the variants that have circulated in human populations since 1918) are depicted in red. Each HA subtype's stem domain is more similar to the other subtypes within its group than to any subtype in the opposing group, consistent with the observed imprinting pattern operating within, but not between, HA groups.

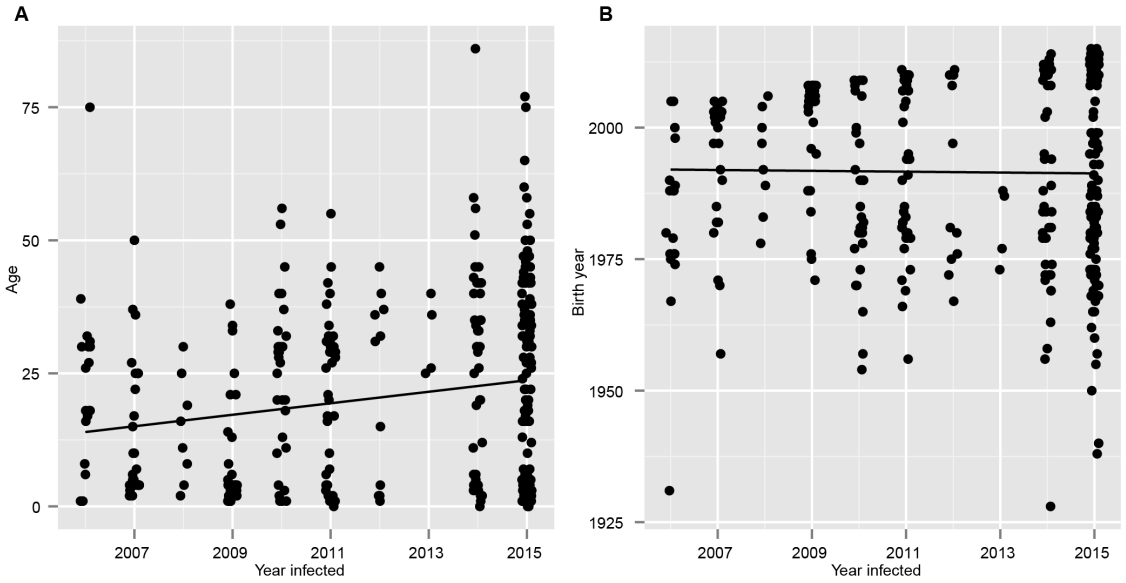

Fig. S2. Trends in age and birth year of H5N1 cases over time. For 361 H5N1 cases observed in Egypt from 2006-2015, (**A)** Spearman's rank correlation showed a significant positive association ($p = 0.0003$, one-sided test) between patient age and year of case observation. Points are jittered around the case observation year, and a least-squares trend line is shown. (**B)** Using the same test, no significant association was found for patient birth year. In support of the HA imprinting hypothesis, these results show that birth year is a more consistent predictor of severe infection risk than age-specific risk factors.

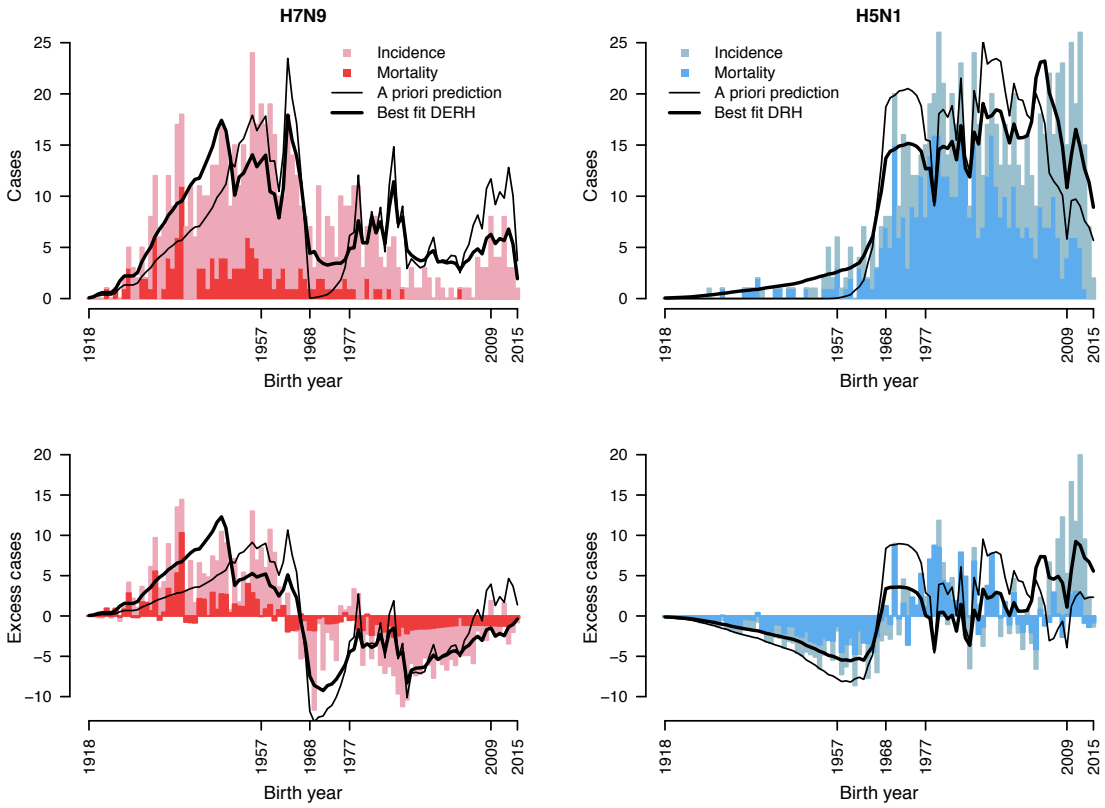

Fig. S3: Model fits to observed data. H7N9 and H5N1 data (bars) are shown with predictions from the best model fit (bold line). For comparison with Fig. 2, *a priori* predictions based on demography and HA imprinting alone (thin line) are also shown.

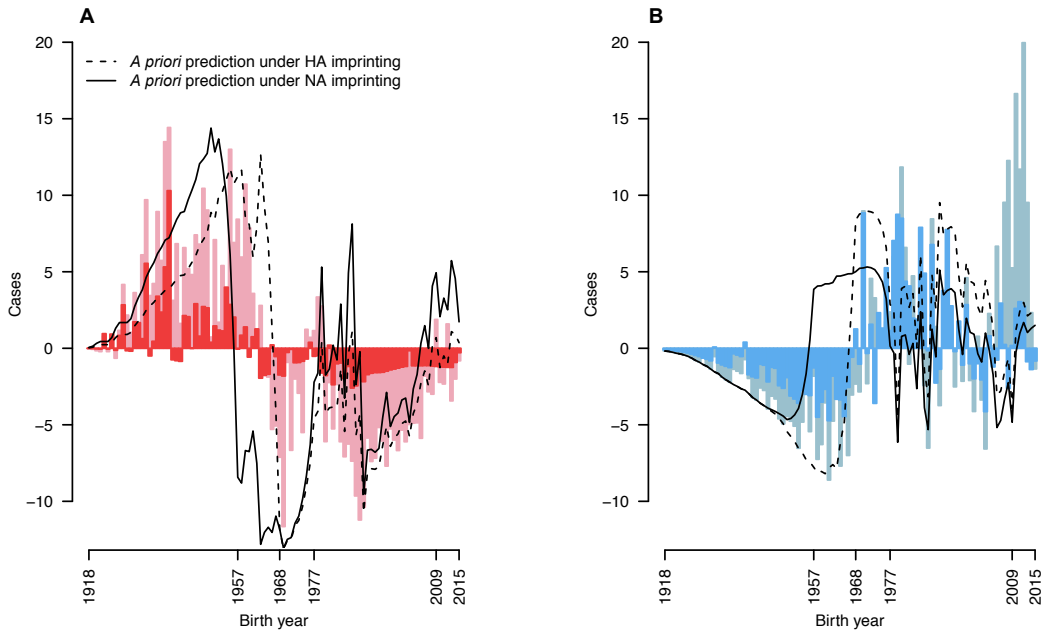

Fig. S4. Comparison of NA and HA imprinting hypotheses to data. (**A**) H7N9. (**B**) H5N1. Bars show incidence (light colors) and mortality (dark colors) normalized to demography as in Figure 2C, D. Overlaid lines show the *a priori* prediction based on HA imprinting (dashed line) or NA imprinting (solid line). During the period from 1957 to 1968 the NA imprinting prediction clearly fails to match observed incidence of excess severe infection or death from H7N9 or H5N1. Moreover, our modeling analysis indicates HA imprinting, not NA imprinting, is the dominant effect driving H5N1 and H7N9 severity patterns (see Table S2).

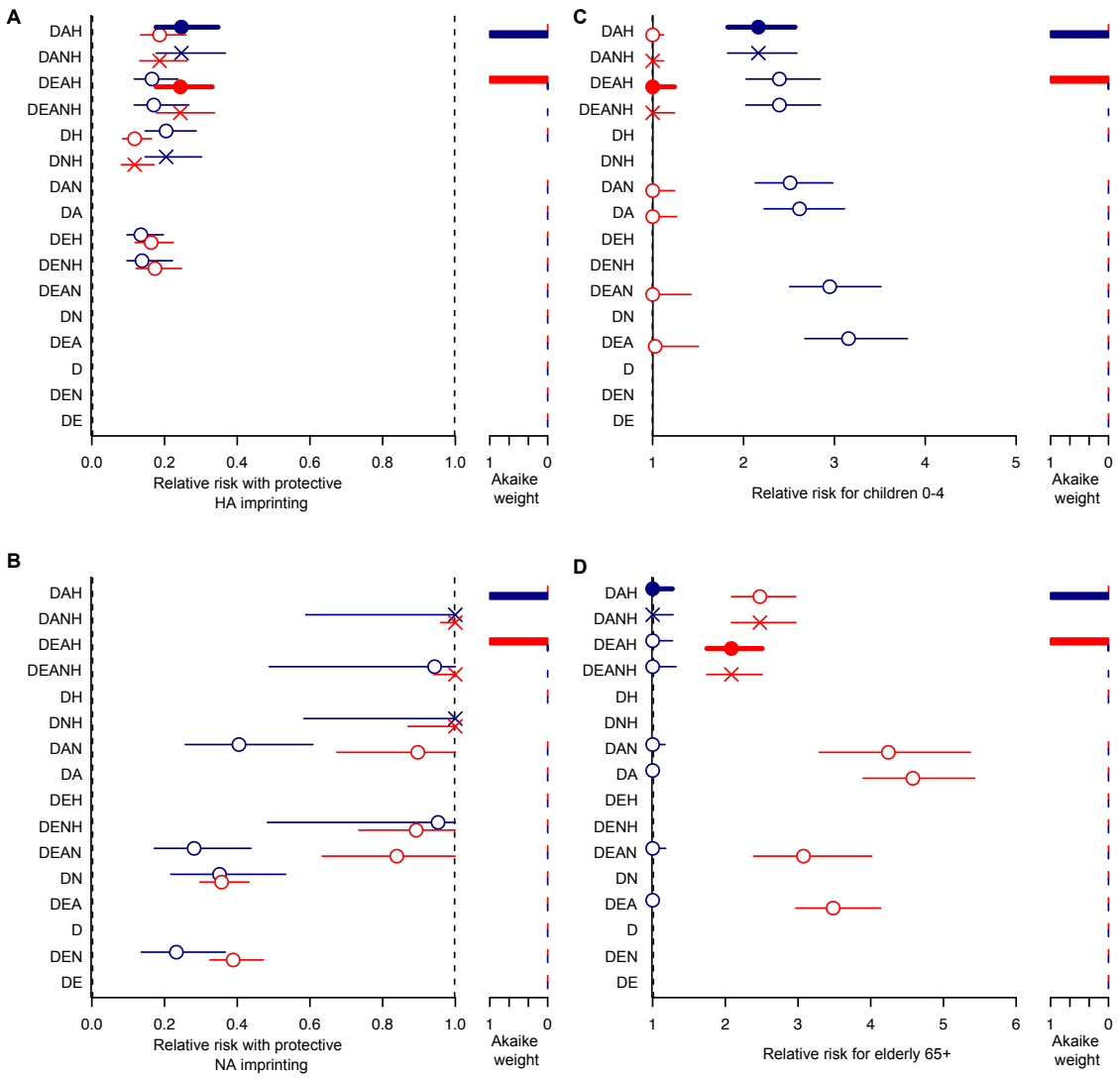

Fig. S5: Parameter estimates for all models of H5N1 and H7N9 incidence. Maximum likelihood estimates and 95% likelihood profile CIs for parameters (with the 95% threshold determined using likelihood ratios) (**A**) H_m (**B**) N_m (**C**) A_c and (**D**) A_e, as fit to H5N1 (blue) and H7N9 (red) incidence data. Parameters and model abbreviations are described in Table S1, and Methods. Demography, D, is included in all models. Additional tested factors include poultry exposure risk, E, age-based risk of severe morbidity in children and the elderly, A, NA imprinting, N, and HA imprinting, H. Dashed lines indicate boundary values imposed on parameters. Models are listed from top to bottom in order of decreasing model support, as fit to H5N1 data. Bar plots at right show Akaike weights, and the best model is shown with a filled symbol and bold line; all preferred models have definitive statistical support with Akaike weights > 0.99 (Table S2). In some cases, the MLE for parameter N_m was 1, indicating no NA imprinting effect, and the model with added factor N was identical to the model containing all the same factors except N. These degenerate models are represented with X's, and were excluded from Akaike weight calculations.

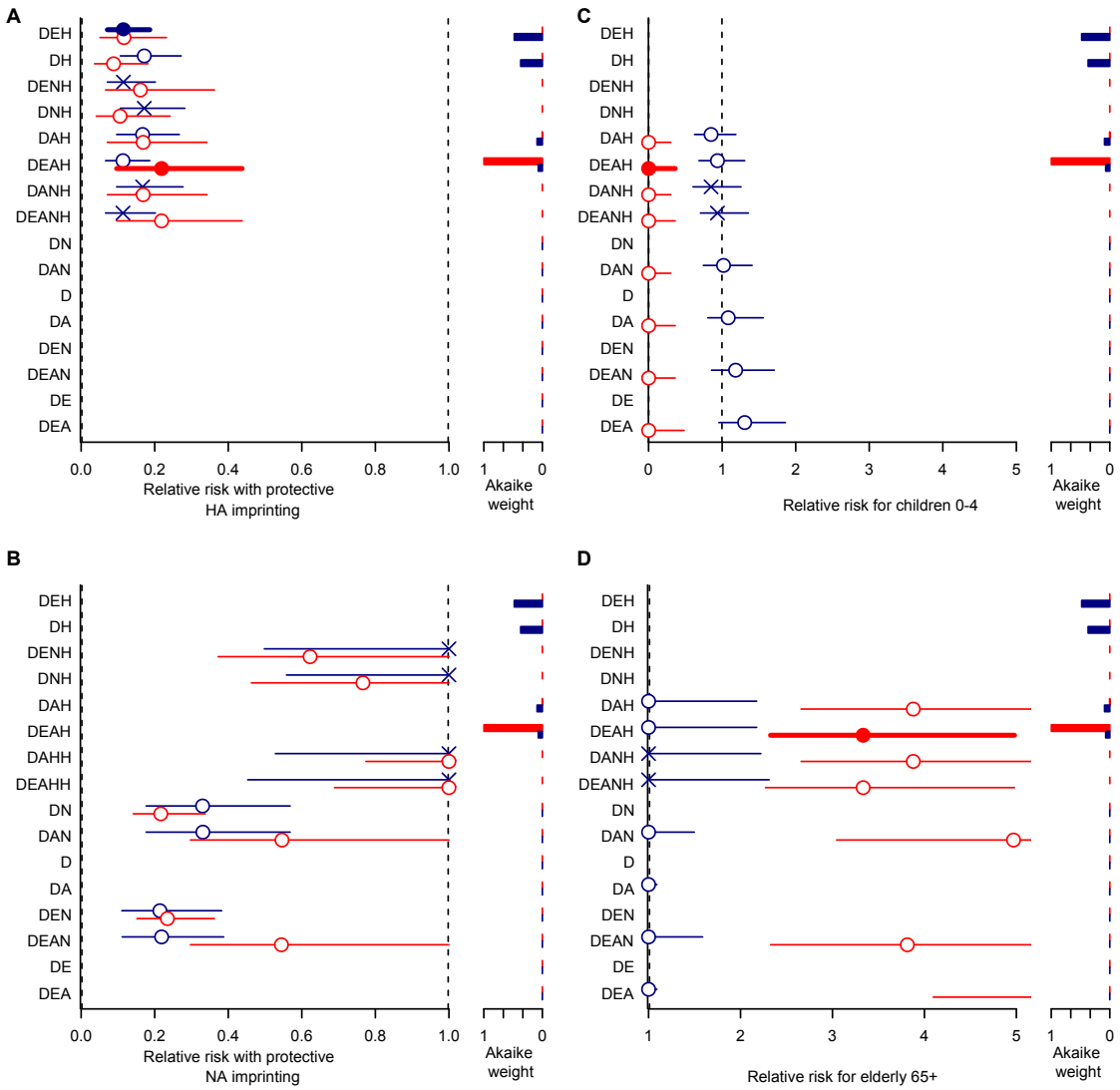

Fig. S6: Parameter estimates for all models of H5N1 and H7N9 mortality. Maximum likelihood estimates and 95% likelihood profile CIs for parameters (**A**) H_m (**B**) N_m (**C**) A_c and (**D**) A_e, as fit to H5N1 (blue) and H7N9 (red) mortality data. Parameters and model abbreviations are described in Table S1, and Methods. Formatting is as in Fig. S5. For H7N9, which is less pathogenic in birds and humans than H5N1, DEAH is the definitive preferred model for both infection and mortality, with Akaike weights > 0.99 in both cases. However, for H5N1, which is more pathogenic in birds and humans, no single mortality model is definitively preferred. Rather, we found some statistical support (Akaike weights > 0.05) for all mortality models that include HA imprinting (Table S2).

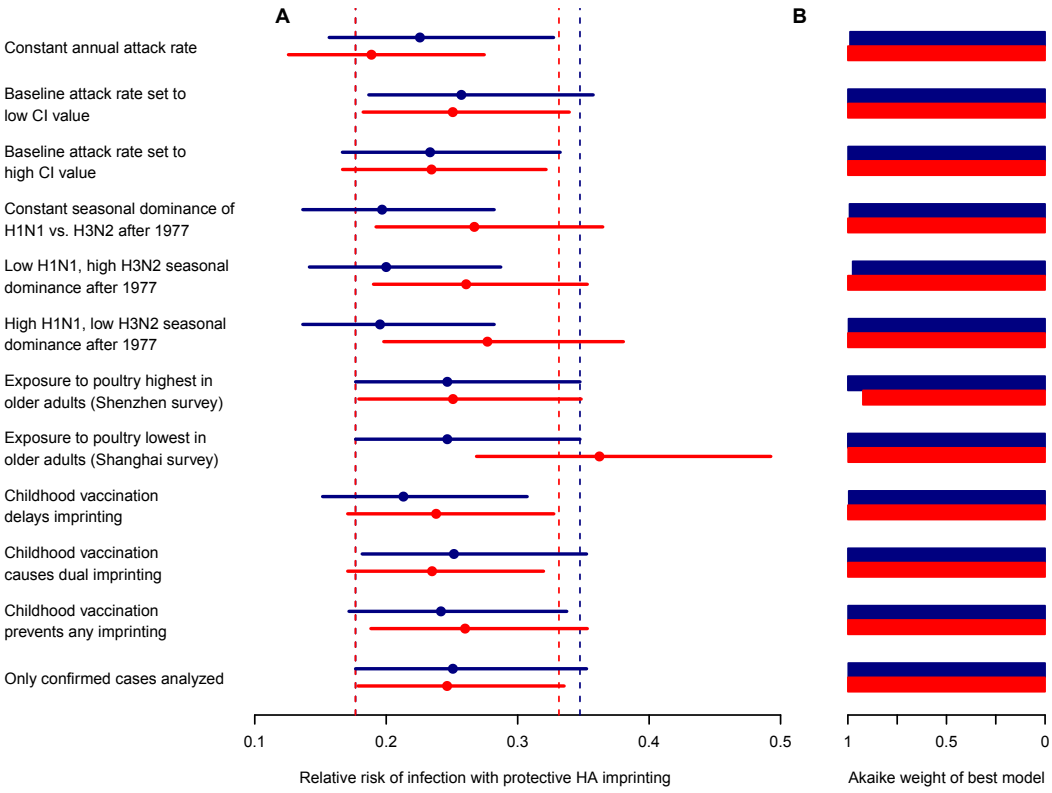

Fig. S7: Sensitivity analyses. We tested the robustness of H_m parameter estimates (Table S1) and model selection results for twelve variations on our standard model formulation (Methods). (**A)** Maximum likelihood estimates and 95% likelihood profile CIs for parameter H_m, as fit to incidence data using the best incidence model for each subtype (DAH for H5N1, in blue, and DEAH for H7N9, in red). Dashed lines show 95% CIs on H_m estimates from the preferred model, as presented in the main text analysis. (**B)** Akaike weights for models DAH (H5N1, blue) and DEAH (H7N9, red). These models remain strongly supported throughout all sensitivity analyses, with Akaike weights > 0.98 in all cases but one. The lowest Akaike weight was 0.92.

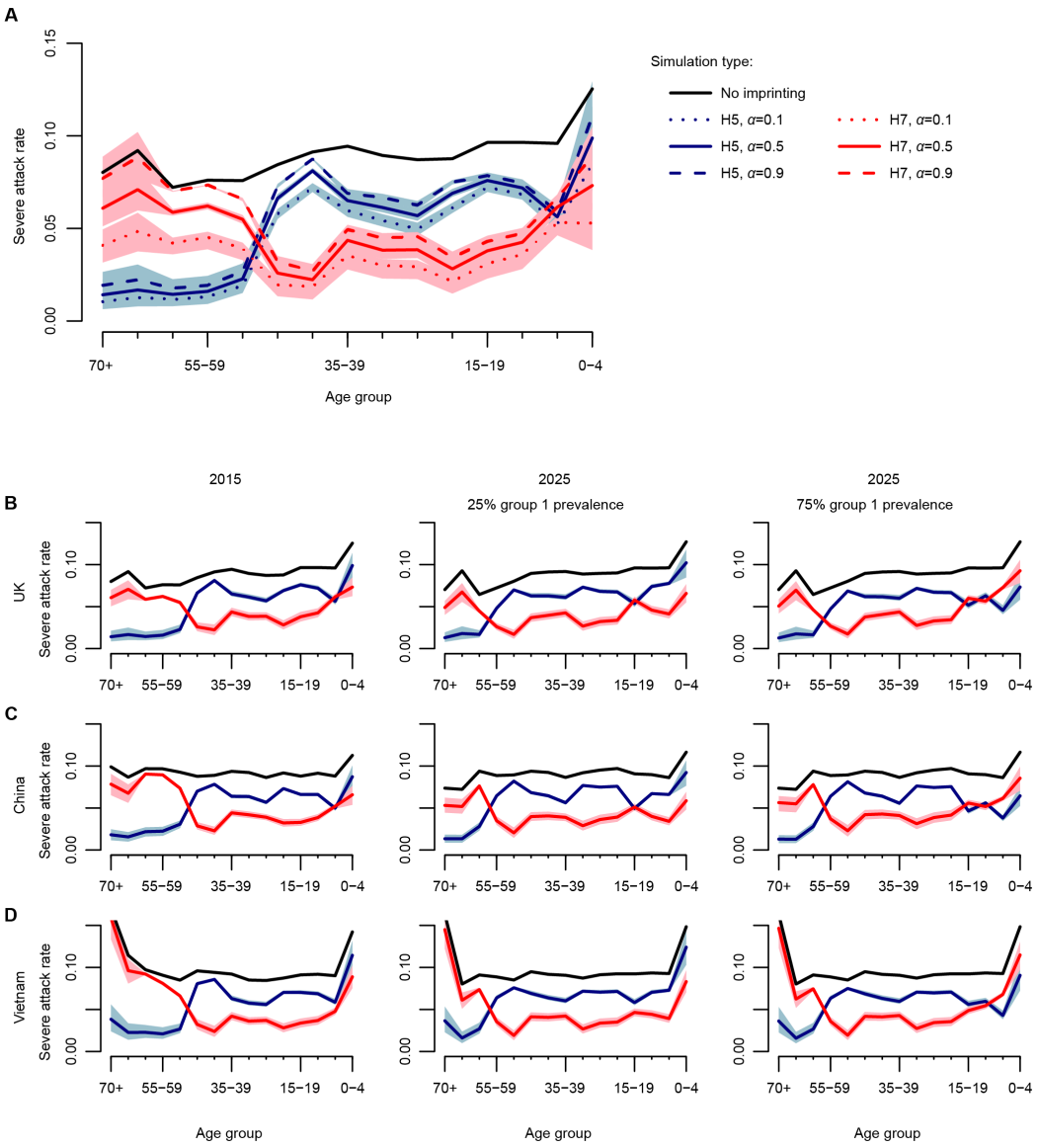

Fig. S8: Projected age-structured severe attack rates during hypothetical future H5 (blue) and H7 (red) IAV pandemics. Simulations assume country-specific demography and age-structured mixing, HA imprinting, and age-based risk groups (Supplementary Text). Colored lines show the average, and shaded regions include 95% of 100 simulated outcomes. For comparison, the severe attack rate in an IAV pandemic with no HA imprinting is also shown (black). All simulations use $R_0 = 2.5$. **(A)** Illustration of how changing the infectiousness of partially protected individuals (α), relative to unprotected individuals, affects the age-structured severe attack rate in a 2015 UK IAV pandemic. **(B-D)** Results for three countries in 2015 and 2025 when α=0.5. Two scenarios are considered for seasonal influenza circulation between 2015 and 2025: 25% group 1 IAV and 75% group 1 IAV.

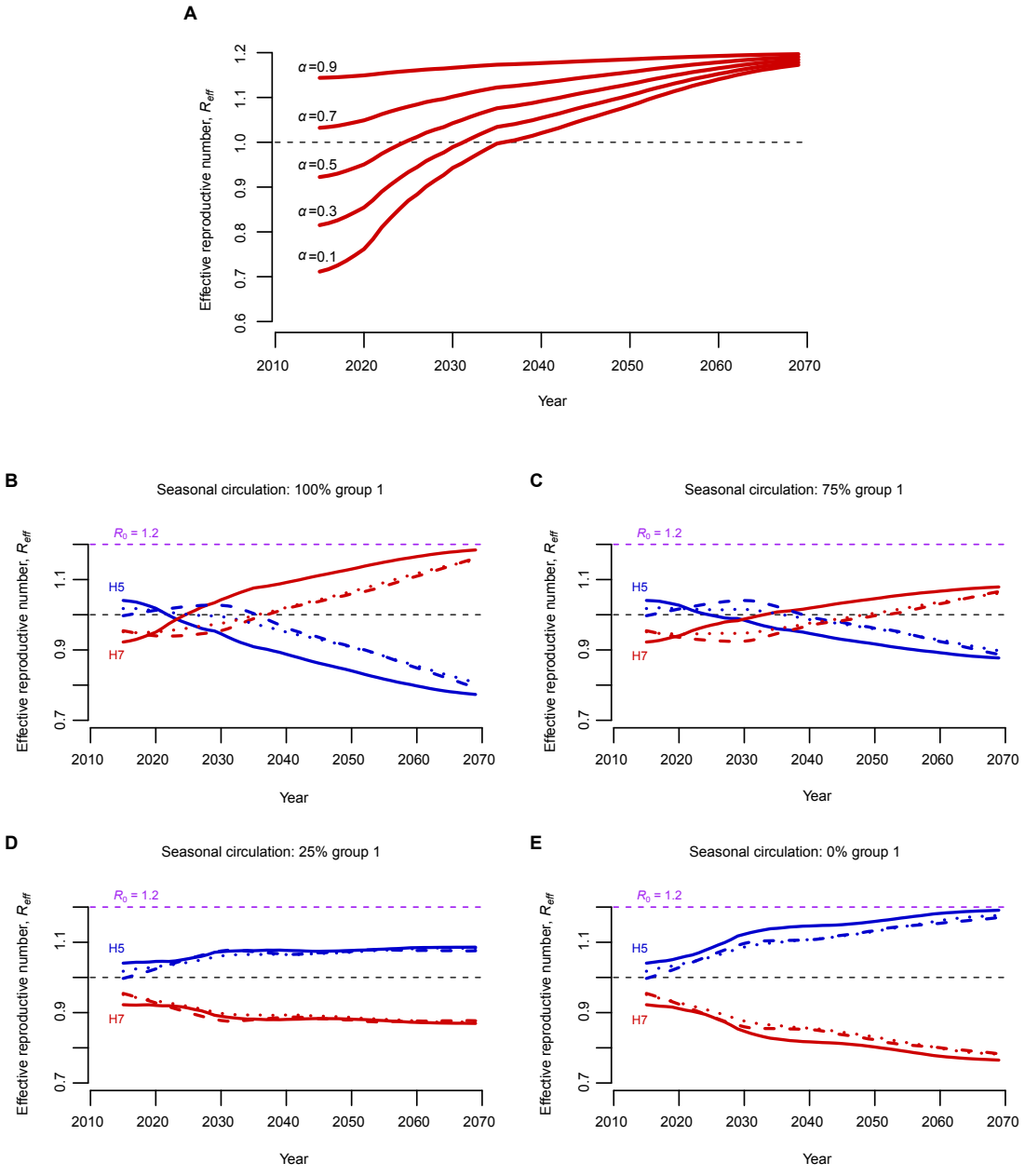

Fig. S9: Projections of R_{eff} through time. **(A)** Projections of R_{eff} for an H7 IAV with R_0 = 1.2 under different assumptions regarding the infectiousness of protected individuals (α). Projections are in the UK assuming 100% group 1 seasonal circulation after 2015. **(B-E)** Projections of how the R_{eff} for a hypothetical H5 (blue) and H7 (red) IAV with R_0 = 1.2 and α=0.5 would change through time in the UK (solid line), China (dashed line), and Vietnam (dotted line) under four different post-2015 seasonal group 1 IAV circulation scenarios. Although general trends are consistent across countries, different demographic age structures and mixing patterns result in notable differences in the exact R_{eff} trajectory of each country.

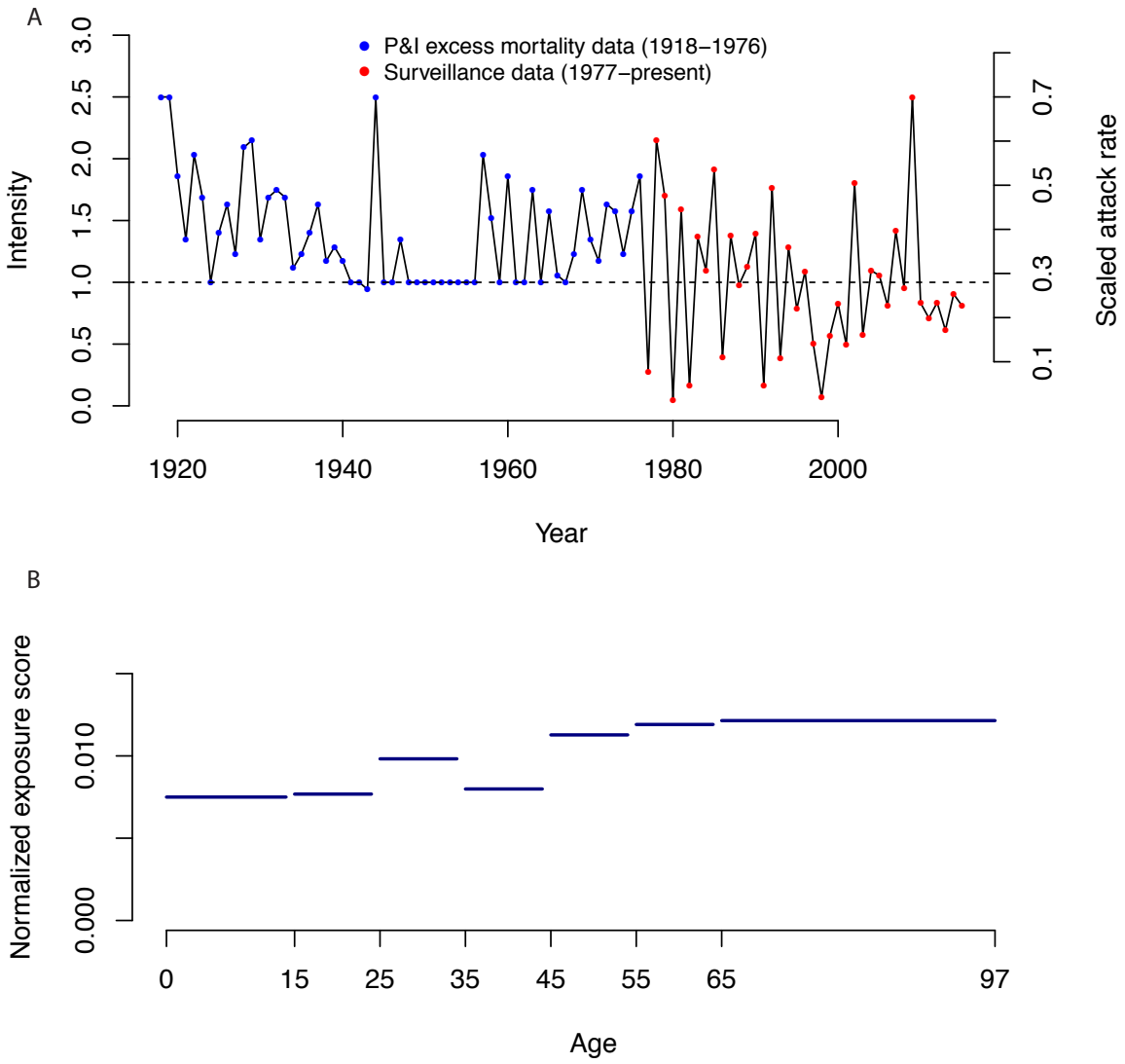

Fig. S10: Model inputs. **(A)** Index representing annual intensity of seasonal influenza circulation from 1918-2015. Right axis shows scaled annual attack rates on naïve children, which correspond to the intensity scores at left. As described in Supplementary Text, section 4, this index modulates the annual attack rate on children in reconstructions of HA and NA imprinting patterns. Blue points spanning 1918-1976 represent pneumonia & influenza excess mortality data, and hence are restricted to non-negative values. **(B)** Index of poultry exposure frequency by age group in humans, described in Methods. This index informs factor E in model comparison.

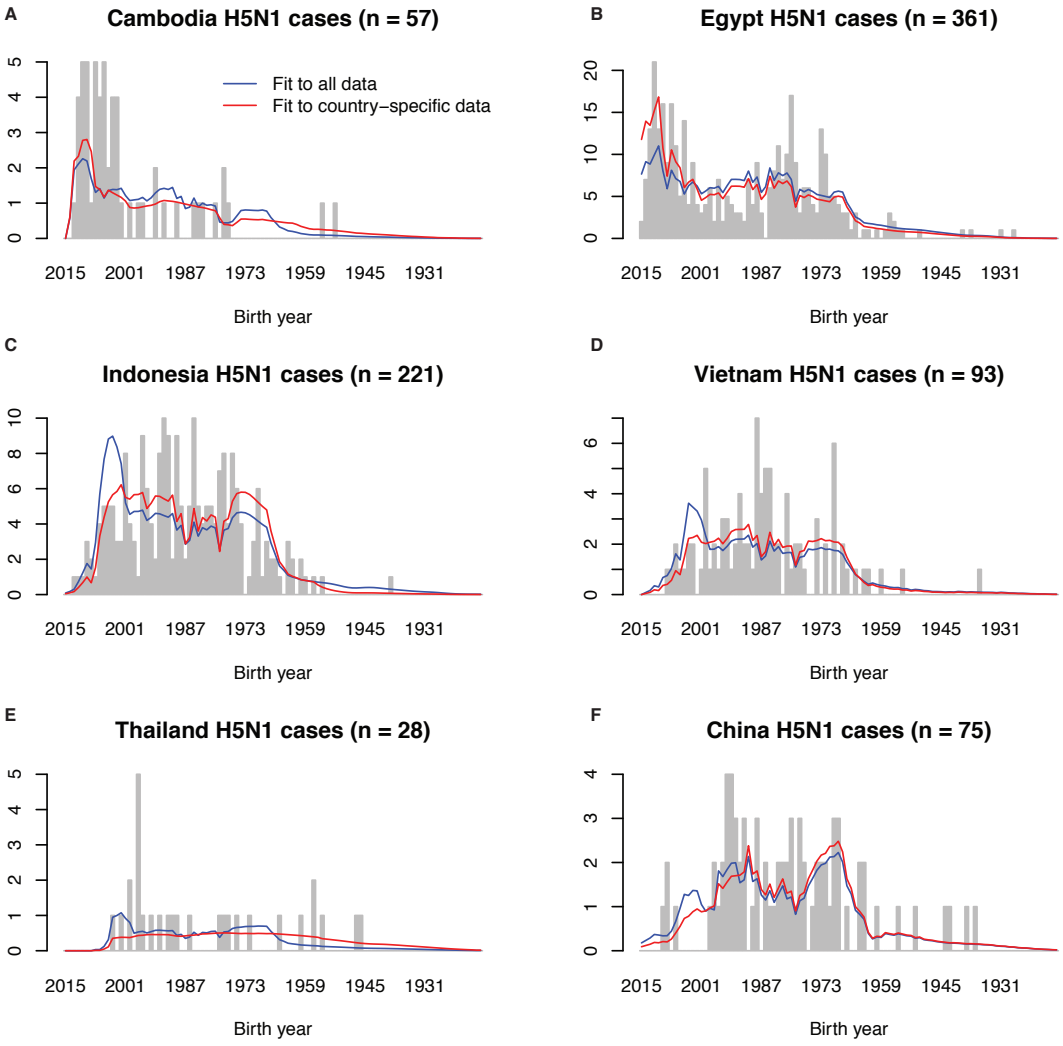

G

	N	Best model	H_m (95% CI)	N_m (95% CI)	A_c (95% CI)	A_e (95% CI)
Cambodia	57	DR			3.25 (1.72-5.61)	1.00 (1.00-2.15)
China	75	D**H**	0.24 (0.10-0.50)			
Egypt	361	DER**H**	0.20 (0.11-0.33)		3.80 (3.02-4.80)	1.00 (100-2.15)
Indonesia	221	DN**H**	0.19 (0.07-0.39)	0.24 (0.02-1.00)		
Thailand	28	D				
Vietnam	93	D**H**	0.16 (0.41-0.43)			

Fig. S11: Country-specific model fits and model comparison results. **(A-F)** Birth year distribution of cases from the country of interest (bars) with overlaid predictions from the best model fit to country-specific data (red), or fit to all data (blue). **(G)** Results of model comparison and maximum likelihood estimation for country-specific data. For Cambodia and Thailand, the second best models (DRH and DH) included HA imprinting effects, and were statistically indistinguishable from the best model with ΔAIC of 0.47 and 0.45.

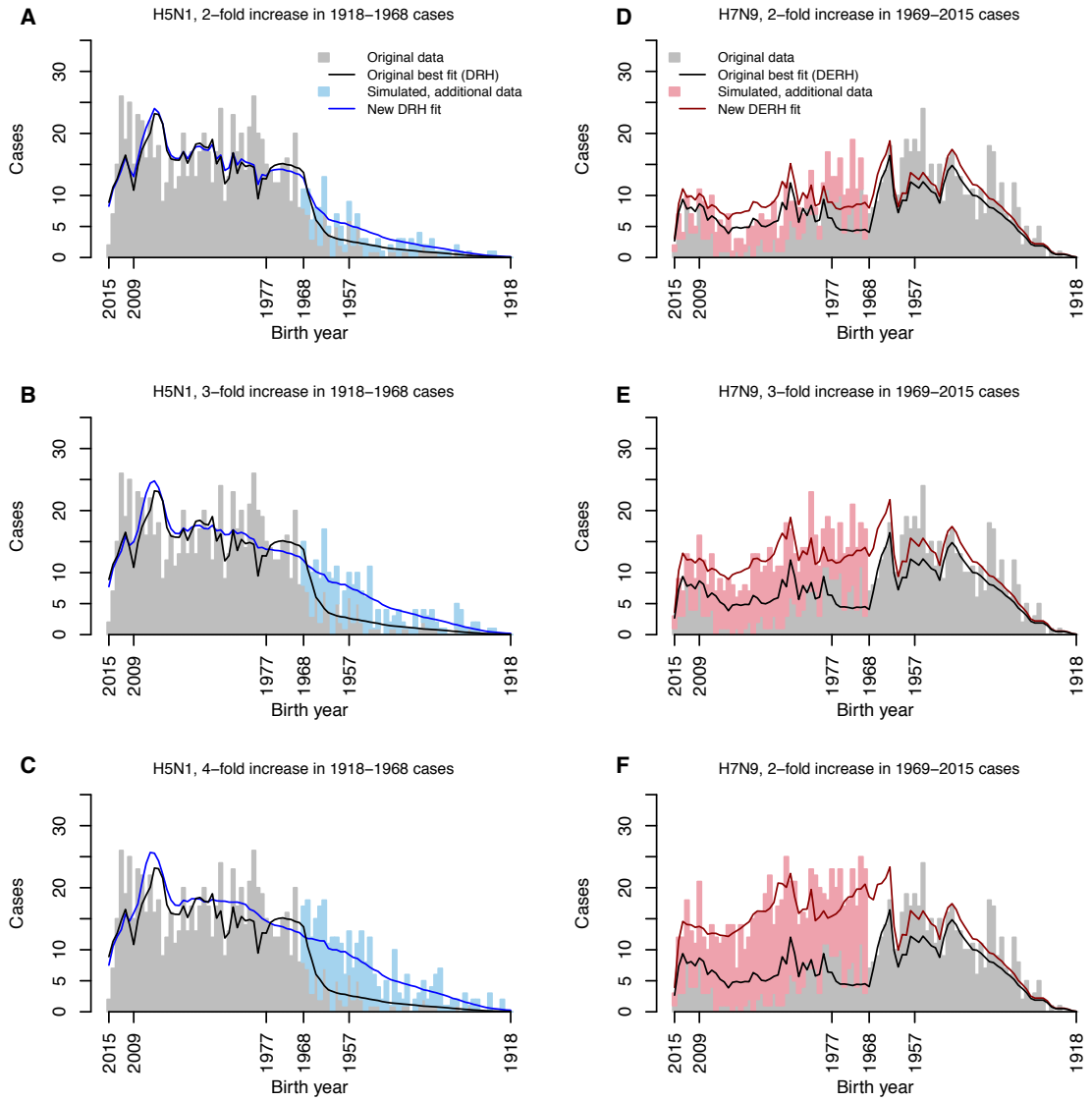

Fig. S12: Robustness to biased case ascertainment. Panels show results of representative simulations showing effects of a worst-case-scenario case ascertainment bias based on birth year (as described in Supplementary Text section 7). We increased the number of cases observed in underrepresented birth cohorts (1918-1968 for H5N1, 1969-2015 for H7N9) by 2-fold **(A, D)**, 3-fold **(B, E)**, or 4-fold **(C, F)** to systematically degrade the strongest signal of HA imprinting in the data. Even with these simulated, 'perfectly bad' biases, our core results were robust up to the 3-fold level for H5N1 and the 4-fold level for H7N9. Note that the gap between model predictions and observed case numbers for H7N9 for birth years leading up to 1968 **(E, F)** arises from lags in imprinting: many individuals born just before the 1968 pandemic actually did imprint on the group 2 1968 virus, but were not included in our data augmentation scheme. Because the estimated protective effect of imprinting is weakened under 3-fold and 4-fold scenarios, the best fit models in these scenarios do not capture the partially protected status of these cohorts.

Tables and legends

Model factors		
Abbreviation	Model factor	Description
D	Demography	Demography modulates the probability, p_{cyi}, that an infection occurs in a particular birth year, i, based on the proportion of the population in country c, in year y, that was born in that year. Demography serves as the null model, and is included as a factor in all models tested.
E	Exposure to poultry	Exposure to poultry is a factor that modulates p_{yci} based on age-specific poultry exposure rates, as informed by data collected in China.
A	Age-based risk	Age-based risk is a factor that allows children ages 0-4, or the elderly ages 65+ to experience elevated risk of severe morbidity, mortality, or increased case ascertainment. This factor modulates p_{yci} via parameters A_c and A_e, as described below.
H	HA imprinting	HA imprinting is a factor that allows those with protective HA imprinting to experience decreased risk of severe infection or mortality, relative to all others. This factor modulates p_{yci} via parameter H_m, as described below.
N	NA imprinting	NA imprinting is a factor that allows those with protective NA imprinting to experience decreased risk of severe infection or mortality, relative to all others. This factor modulates p_{yci} via parameter N_m, as described below.

Model parameters			
Parameter	Description	Constraints	Interpretation of constraints
H_m	Relative susceptibility of those with group-matched (protective) first hemagglutinin exposures.	$0 \leq H_m \leq 1$	0 indicates full protection 1 indicates no additional protection
N_m	Relative susceptibility of those with group-matched (protective) first neuraminidase exposures.	$0 \leq N_m \leq 1$	0 indicates full protection 1 indicates no additional protection
A_c	Relative risk of severe infection/case detection bias for young children (ages 0-4)	$A_c \geq 1$*	1 indicates no elevated risk >1 indicates elevated risk
A_e	Relative risk of severe infection/case detection bias for the elderly (ages 65+)	$A_e \geq 1$	1 indicates no elevated risk >1 indicates elevated risk

Table S1. Summary of model factors and free parameters.

*For models analyzing mortality risk, we changed this constraint to: $A_c \geq 0$, allowing the data to indicate whether young children were more or less likely to die from their infections than the reference age group (see Methods).

	H_m (95% CI)	N_m (95% CI)	A_c (95% CI)	A_e (95% CI)	ΔAIC	Akaike weight
H5N1 incidence						
DAH	0.25 (0.18-0.35)		2.16 (1.83-2.57)	1.00 (1.00-1.27)	0	1.00
DANH*	0.25 (0.18-0.37)	1.00 (0.59-1.00)	2.16 (1.82-2.59)	1.00 (1.00-1.28)	2	
DEAH	0.17 (0.12-0.24)		2.39 (2.03-2.84)	1.00 (1.00-1.27)	15.35	4.65E-04
DEANH	0.17 (0.12-0.27)	0.94 (0.49-1.00)	2.39 (2.03-2.85)	1.00 (1.00-1.32)	17.32	1.74E-04
DH	0.20 (0.15-0.29)				69.81	9.50 E-16
DNH*	0.20 (0.15-0.30)	1.00 (0.58-1.00)			71.18	
DAN		0.40 (0.26-0.61)	2.51 (2.13-2.98)	1.00 (1.00-1.17)	73.58	1.05E-16
DA			2.62 (2.23-3.11)	1.00 (1.00-1.06)	96.34	1.20E-21
DEH	0.13 (0.10-0.20)				103.31	3.69E-23
DENH	0.14 (0.10-0.22)	0.95 (0.48-1.00)			105.29	1.37E-23
DEAN		0.28 (0.17-0.44)	2.95 (2.51-3.51)	1.00 (1.00-1.18)	136.99	1.79E-30
DN		0.35 (0.22-0.53)			172.30	3.84E-38
DEA			3.16 (2.67-3.80)	1.00 (1.00-1.05)	182.33	2.56E-40
D					203.81	5.52E-45
DEN		0.23 (0.14-0.37)			269.81	2.57E-59
DE					331.46	1.06E-72
H7N9 incidence						
DEAH	0.24 (0.18-0.33)		1.00 (1.00-1.24)	2.08 (1.74-2.51)	0	1.00
DEANH*	0.24 (0.18-0.34)	1.00 (0.94-1.00)	1.00 (1.00-1.24)	2.08 (1.74-2.51)	2	
DAH	0.19 (0.13-0.26)		1.00 (1.00-1.12)	2.47 (2.09-2.97)	42.87	4.90E-10
DANH*	0.19 (0.13-0.26)	1.00 (0.96-1.00)	1.00 (1.00-1.12)	2.47 (2.09-2.97)	44.87	
DEH	0.16 (0.12-0.22)				61.59	4.23E-14
DENH	0.17 (0.12-0.25)	0.89 (0.73-1.00)			62.26	3.02E-14
DEA			1.03 (1.00-1.50)	3.48 (2.97-4.14)	106.94	6.00E-24
DEAN		0.84 (0.63-1.00)	1.00 (1.00-1.42)	3.07 (2.39-4.02)	107.63	4.24E-24
DH	0.12 (0.08-0.16)				138.40	8.83E-31
DNH*	0.12 (0.08-0.17)	1.00 (0.87-1.00)			140.40	
DA			1.00 (1.00-1.26)	4.58 (3.89-5.43)	193.47	9.72E-43
DAN		0.90 (0.67-1.00)	1.00 (1.00-1.24)	4.24 (3.29-5.37)	194.97	4.60E-43
DEN		0.39 (0.32-0.47)			195.62	3.33E-43
DE					297.51	2.49E-65
DN		0.36 (0.30-0.43)			344.49	1.57E-75
D					466.22	5.76E-102
H5N1 mortality						
DEH	0.11 (0.07-0.19)				0.00	0.48
DH	0.17 (0.11-0.27)				0.53	0.37
DENH*	0.11 (0.07-0.20)	1.00 (0.50-1.00)			2.00	
DNH*	0.17 (0.11-0.28)	1.00 (0.56-1.00)			2.53	
DAH	0.17 (0.10-0.27)		0.85 (0.62-1.19)	1.00 (1.00-2.18)	3.41	0.09
DEAH	0.11 (0.07-0.19)		0.94 (0.68-1.31)	1.00 (1.00-2.18)	3.82	0.07
DANH*	0.17 (0.10-0.28)	1.00 (0.53-1.00)	0.85 (0.60-1.26)	1.00 (1.00-2.22)	5.41	
DEANH*	0.11 (0.07-0.20)	1.00 (0.45-1.00)	0.94 (0.70-1.36)	1.00 (1.00-2.31)	5.82	
DN		0.33 (0.18-0.57)			69.22	4.44E-16
DAN		0.33 (0.18-0.57)	1.02 (0.74-1.41)	1.00 (1.00-1.50)	73.21	6.06E-17
D					87.98	3.76E-20
DA			1.08 (0.80-1.56)	1.00 (1.00-1.09)	91.72	5.78E-21
DEN		0.21 (0.11-0.38)			104.04	1.22E-23
DEAN		0.22 (0.11-0.39)	1.18 (0.86-1.71)	1.00 (1.00-1.59)	106.93	2.88E-24
DE					143.27	3.69E-32
DEA			1.31 (0.96-1.86)	1.00 (1.00-1.09)	144.54	1.96E-32
H7N9 mortality						
DEAH	0.22 (0.10-0.44)		0.00 (0.00-0.36)	3.33 (2.33-4.98)	0	1.00
DEANH*	0.22 (0.10-0.44)	1.00 (0.69-1.00)	0.00 (0.00-0.36)	3.33 (2.27-4.98)	2	
DAH	0.17 (0.07-0.34)		0.00 (0.00-0.30)	3.88 (2.66-5.57)	12.05	2.41E-03
DANH*	0.17 (0.07-0.34)	1.00 (0.77-1.00)	0.00 (0.00-0.30)	3.88 (2.66-5.57)	14.05	
DEAN		0.54 (0.30-1.00)	0.00 (0.00-0.36)	3.81 (2.33-6.68)	20.34	3.83E-05
DEA			0.00 (0.00-0.48)	5.78 (4.10-8.24)	21.45	2.19E-05
DAN		0.55 (0.30-1.00)	0.00 (0.00-0.30)	4.97 (3.05-8.90)	40.94	1.29E-09
DA			0.00 (0.00-0.36)	7.51 (5.31-10.67)	42.03	7.47E-10
DENH	0.16 (0.07-0.36)	0.62 (0.37-1.00)			49.16	2.11E-11
DEH	0.12 (0.05-0.23)				51.14	7.84E-12
DEN		0.23 (0.15-0.36)			68.32	1.45E-15
DH	0.09 (0.04-0.18)				79.85	4.56E-18
DNH*	0.11 (0.04-0.24)	0.77 (0.46-1.00)			80.60	3.13E-18
DN		0.22 (0.14-0.34)			110.60	9.62E-25
DE					116.94	4.03E-26
D					165.02	1.46E-36

Table S2. Incidence and mortality model results.

*Maximum likelihood model was identical to the model including all the same factors except N, and excluded from Akaike weight calculations.

Additional Data S1-S3

Data table S1. Details of H5N1 cases reported from 2003-Sept. 2006, and from Sept. 2010- Nov. 2015, in .xls format. Cases occurring in 1997 and from Sept. 2006-Aug. 2010 are available in previously published line lists. See Chan, P. K. S. *Clin*. *Infect*. *Dis*. **34,** S58–S64 (2002)., and Fiebig, L. *et al*. *Eurosurveillance* **16,** 1–10 (2011).

Data table S2. Details of H7N9 cases reported from 16 Oct. 2013 to Nov. 2015. Cases occurring prior to 16 Oct. 2013 are available in a previously published line list (see Data from Kucharski, A. et al. PLoS Curr. Outbreaks (2014). doi:10.5061/dryad.2g43n).

Code S3. A .zip file containing R scripts used to perform maximum likelihood estimation and model comparison. See Read Me file within for details.